TOLLIP promotes durable alveolar macrophage-mediated immunity during *Mycobacterium tuberculosis* infection by resolving cellular stress from lipids.

Sambasivan Venkatasubramanian[1], Courtney Plumlee[2], Kim Dill-McFarland[1], Gemma L. Pearson[3], Sara B. Cohen[2], Anne Lietzke[3], Amanda Pacheco[3], Robyn Pryor[1], Scott A. Soleimanpour[3,4], Matthew Altman[1], Kevin B. Urdahl[2,5], Javeed A. Shah[1,6*].

[1] Department of Medicine, University of Washington, Seattle, WA.

[2] Seattle Children's Research Institute, Seattle, WA.

[3] Department of Internal Medicine, University of Michigan, Ann Arbor, MI.

[4] VA Ann Arbor Healthcare System, Ann Arbor, MI.

[5] Departments of Pediatrics and Immunology, University of Washington, Seattle, WA.

[6] VA Puget Sound Healthcare System, Seattle, WA.

[*] Correspondence: jashah@uw.edu; @ShahLab.

Summary

TOLLIP, a ubiquitin binding protein that controls multiple macrophage functions via endoplasmic reticulum transport and autophagy, is associated with human tuberculosis (TB) susceptibility and immune responses in genetic studies. We investigated how TOLLIP influences immunity during *Mycobacterium tuberculosis* (Mtb) infection in the mouse model. During early infection, *Tollip*$^{-/-}$ mice had reduced mycobacterial burden and increased innate immune responses, but later, *Tollip*$^{-/-}$ mice developed worse disease and many foam cells within their lung infiltrates. The delayed immune impairment was intrinsic to alveolar macrophages, associated with cellular stress, and accompanied by lipid accumulation. Further, this phenotype was reproducible with administration of exogenous lipids. Thus, TOLLIP expression in alveolar macrophages is necessary for durable protection from prolonged Mtb infection by resolving lipid-induced cellular stress. These descriptions define a critical role for TOLLIP as part of the lipid-induced ER stress response, which is responsible for Mtb progression during post-primary infection.

Keywords: TOLLIP, tuberculosis, macrophages, foam cells, innate immunity, unfolded protein response, cellular homeostasis, lipid metabolism, autophagy, ER stress

Introduction

Toll-Interacting Protein (TOLLIP) is a selective autophagy receptor and endosomal sorting protein that was initially identified as a TLR and IL-1R binding protein (Burns et al., 2000) that also chaperones protein aggregates to the autophagosome via ER transport (Jongsma et al., 2016; Lu et al., 2014). TOLLIP's immune regulatory and homeostatic functions act in competition, as excess protein aggregates prevent TOLLIP from influencing innate immune responses (Pokatayev et al., 2020). In prior studies, we found that a functionally active single nucleotide polymorphism upstream of the TOLLIP transcriptional start site that results in diminished TOLLIP gene expression in monocytes is associated with increased risk for pulmonary and meningeal TB, increased innate immune responses after Mtb infection, and diminished BCG-specific T cell responses in South African infants (Shah et al., 2016; Shah et al., 2017). Thus, the mechanism by which TOLLIP influences Mtb susceptibility remains poorly defined, especially during chronic phases of infection. We evaluated how TOLLIP influences pulmonary immune responses to Mtb infection and TB severity over time using *Tollip*$^{-/-}$ mice.

The impact of autophagy on Mtb pathogenesis is dramatic but incompletely understood. After IFNγ activation, autophagy contributes to host defense within murine macrophages by trafficking Mtb to autophagolysosomes for destruction, but this only represents a partial contribution to Mtb clearance (Gutierrez et al., 2004; Ouimet et al., 2016). Autophagy also dampens innate immune responses, including inflammasome and TLR activity (Matsuzawa-Ishimoto et al., 2018), and the autophagy regulator Atg5 controls neutrophil-induced tissue destruction and immunopathology after Mtb infection (Kimmey et al., 2015; Levine et al., 2011). Autophagy is also induced to clear misfolded proteins and excess lipid, which is a component of

the ER stress response and an important mechanism for maintaining cellular function over time (Grootjans et al., 2016). ER stress induces multiple adverse effects in immune cells, but its effects on Mtb-infected macrophages are not completely understood.

Unrelieved ER stress induces multiple adverse effects in macrophages that may influence Mtb immune responses and pathogenesis. Stressed macrophages develop inflammatory overreaction to bacterial products and TNF, which can worsen outcomes from TB infection (Kaser et al., 2008; Roca et al., 2019). ER stress also diminishes protein translation, induces cell cycle arrest, and impairs glycolysis, which are each important for Mtb control (Mizushima and Komatsu, 2011; Russell et al., 2019). Last, ER stress strongly influences macrophage polarization and differentiation, which may influence Mtb outcomes (Oh et al., 2012). In this study, we found that TOLLIP participates in lipid clearance from alveolar macrophages (AM) and is an important component of the ER stress response during prolonged Mtb infection in this macrophage subtype. These data support targeting of TOLLIP as a strategy to overcome Mtb-induced lipid accumulation and stress and as a way to maintain macrophage homeostasis during chronic Mtb disease.

Results

Tollip$^{-/-}$ macrophages develop proinflammatory cytokine bias after Mtb infection. In preliminary experiments, we identified a functional single nucleotide polymorphism in the TOLLIP promoter region that was associated with decreased TOLLIP mRNA expression in peripheral blood monocytes and hyperinflammatory cytokine responses after TLR stimulation and Mtb infection (Shah et al., 2016; Shah et al., 2017; Shah et al., 2012). This variant was also associated with increased risk for pulmonary and meningeal TB in genetic studies (Shah et al., 2012). To link

these human genetic observations with our small animal model, we evaluated the functional capacity of *Tollip*$^{-/-}$ macrophages to produce pro- and anti-inflammatory cytokines after TLR stimulation and Mtb infection. We isolated peritoneal macrophages (PEM), plated them *ex vivo* and stimulated them with LPS (TLR4 ligand; 10ng/ml), PAM3 (TLR2/1 ligand; 250ng/ml), or Mtb whole cell lysate (1µg/ml). *Tollip*$^{-/-}$ PEM secreted more TNF than control after all stimulation conditions (**Figure 1A**, LPS p = 0.01, PAM3 p = 0.002, Mtb lysate p = 0.01, n = 9). Conversely, *Tollip*$^{-/-}$ PEM induced less IL-10 than controls (**Figure 1B**, LPS p = 0.01, PAM3 p = 0.02, Mtb lysate p =0.03, n = 9). We infected PEM with live Mtb H37Rv strain (MOI 2.5) overnight and measured TNF, IL-1β and IL-10. After infection, *Tollip*$^{-/-}$ PEM secreted more TNF and IL-1β, while inducing less IL-10 than controls (MOI 2.5) (**Figure 1C-E**; p=0.03, p=0.03, and p=0.02 respectively), which is consistent with macrophage responses observed in human cell lines and genetic variants associated with diminished TOLLIP mRNA transcript (Shah et al., 2017; Shah et al., 2012). Thus, murine TOLLIP recapitulated the functional phenotypes of human TOLLIP after Mtb infection in macrophages.

TOLLIP is required to control Mtb infection. Human studies suggest that TOLLIP variants are associated with TB susceptibility (Shah et al., 2016; Shah et al., 2017; Shah et al., 2012). Further, a functionally active variant in the TOLLIP promoter was associated with decreased TOLLIP mRNA expression in monocytes and increased innate immune responses to Mtb infection, but diminished BCG-specific T cells responses (Shah et al., 2017). Therefore, we evaluated how TOLLIP influenced TB outcomes in the knockout mouse model to elucidate the mechanistic underpinnings of TOLLIP in the immune response to Mtb *in vivo*. We infected *Tollip*$^{-/-}$ mice and littermate controls expressing *Tollip* (WT) with 100 cfu of Mtb H37Rv strain via aerosol and

monitored weight, bacterial colony forming units (CFU), and survival over time (**Figure 2A**). Lung CFU were diminished 2 weeks after infection in *Tollip*$^{-/-}$ mice ($p < 0.009$, $n = 5$; **Figure 2B**). Four weeks post-infection, Mtb bacterial burdens in the lung were diminished in *Tollip*$^{-/-}$ mice compared with controls (**Figure 2C**, n =30 / mouse type; $p < 0.020$, two-sided t-test). 8 weeks post-infection, this phenotype reversed and *Tollip*$^{-/-}$ mice developed increased bacterial burden ($p=0.0011$, two-sided t-test) and beyond. By 180 days, lung bacterial burdens were increased ten-fold in *Tollip*$^{-/-}$ mice compared to controls ($p = 0.03$, t-test; overall difference in groups, $p = 0.004$, mixed effects model comparing, genotype, time, and TOLLIP expression). Similarly, we found extrapulmonary dissemination of Mtb was delayed in *Tollip*$^{-/-}$ mice, as we were unable to culture Mtb from of 3/5 spleens (**Figure 2D**, $p = 0.06$, two-sided t-test). Further, four weeks after infection, bacterial load was decreased in the spleens of *Tollip*$^{-/-}$ mice, but we observed increased bacterial burden in the spleen after 8 weeks and onward (**Figure 2E**, $p = 0.0092$, 2-way ANOVA comparing time and genotype). *Tollip*$^{-/-}$ mice met criteria for euthanasia a median of 228 days after infection (**Figure 2F**; $p < 0.0001$, $n = 10$ / group, Mantel-Cox test), whereas WT mice did not lose weight and survived over 250 days after infection. *Tollip*$^{-/-}$ mice lost weight beginning approximately 180 days post-infection as well (**Figure 2G**, $p < 0.0001$, 2-way ANOVA accounting for genotype and time). Histopathologic analysis of lung sections also revealed differences between early and late immune responses in *Tollip*$^{-/-}$ mice. Although *Tollip*$^{-/-}$ and WT mice developed qualitatively similar inflammatory lesions four weeks post-infection, by 8 weeks post-infection, *Tollip*$^{-/-}$ mice displayed increased numbers of cellular structures with a foamy appearance within infiltrates, consistent with lipid-laden “foamy” macrophages (**Figure 2H**). Taken together, *Tollip*$^{-/-}$ mice exhibit early resistance to Mtb infection during the first 2-4 weeks, which might be predicted by the enhanced inflammatory response of *Tollip*$^{-/-}$

macrophages. However, paradoxically, during chronic stages of Mtb infection their susceptibility is reversed and *Tollip*$^{-/-}$ mice exhibit higher bacterial burdens than WT controls.

Because TOLLIP is ubiquitously expressed (Consortium, 2015), we generated reciprocal bone-marrow chimeras to assess whether TOLLIP's expression in hematopoietic or non-hematopoeitic cells is required for immunity against Mtb. Lung bacterial burdens were assessed in mice infected with Mtb 8 weeks prior (**Figure 2G**). Consistent with our results in non-chimeric mice (**Figure 2B**), *Tollip*$^{-/-}$ bone marrow → *Tollip*$^{-/-}$ mice exhibited higher lung bacterial burdens that WT → WT controls. Importantly, *Tollip*$^{-/-}$ → WT chimeras had elevated bacterial burdens like *Tollip*$^{-/-}$ → *Tollip*$^{-/-}$ controls, whereas bacterial burdens in WT → *Tollip*$^{-/-}$ were not significantly different than WT → WT controls. These data suggest a specific role for TOLLIP in radiosensitive hematopoietic cells during Mtb infection.

TOLLIP deficiency induces increased intracellular Mtb burden in AM during chronic infection. Having shown that TOLLIP expression is required in hematopoietic cells for Mtb immunity, we next sought to identify the specific hematopoietic cell types in which it was essential. In prior studies, we showed that TOLLIP deficiency promotes diminished Mtb replication within macrophages *in vitro*, using early time points exclusively, which correlated with its role in diminishing proinflammatory cytokine responses (Shah et al., 2016; Shah et al., 2019). However, given the opposing results in both human genetic studies and mouse infectious challenge, we investigated whether TOLLIP was required for Mtb control in distinct pulmonary macrophages within the lung over the disease course. We infected *Tollip*$^{-/-}$ and WT mice with Mtb expressing an mCherry fluorescent reporter (50-100 CFU) via aerosol and four and eight weeks after

infection, we measured lung myeloid cell populations and the proportion of cells infected with Mtb using an adaptation of recently devised gating strategies (**Figure S1,** (Cohen et al., 2018; Guilliams et al., 2013)). We found no difference in the proportion of AM (CD11c+SiglecF+), monocyte-derived macrophages (MDM; SiglecF-CD11b+CD11c+MHCII+), interstitial macrophages (IM; SiglecF-CD11b+CD11c-MHCII+), neutrophils (PMN; SiglecF-CD11b+Ly6G+), or dendritic cells (DC; SiglecF-CD11b-CD11c+MHCII+) found in the lung between WT and *Tollip*$^{-/-}$ mice during the course of Mtb infection (**Figure 3A-B**). When we assessed the infected cells, however, we observed a lower percentage of mCherry+ AM and PMN infected with Mtb in *Tollip*$^{-/-}$ mice, compared to WT mice four weeks post-infection (**Figure 3C**, $p = 0.01$ and $p = 0.02$, respectively; $n = 5$). By eight weeks, however, there was a reversal and a significantly greater proportion of Mtb-infected AM and MDM from *Tollip*$^{-/-}$ mice (**Figure 3D**, $p = 0.03$ and $p = 0.01$, respectively). Thus, although the overall proportion of myeloid populations were similar in WT and *Tollip*$^{-/-}$ mice, some myeloid cell subtypes, including AM, were relatively less infected at early timepoints, and relatively more infected at later timepoints.

TOLLIP deficiency induces and maintains increased NOS2 and impaired costimulatory marker activation in lung-resident myeloid cells after Mtb infection. Next, we compared the functional capacity of lung-resident myeloid cells in WT and *Tollip*$^{-/-}$ mice. Four weeks post-infection, Mtb-infected AMs from *Tollip*$^{-/-}$ mice demonstrated significantly increased NOS2 median fluorescence intensity when compared to WT littermates (**Figure 4A**, $p = 0.01$, $n = 5$), and we observed a trend toward increased NOS2 from Mtb infected PMNs in *Tollip*$^{-/-}$ mice. Eight weeks after infection, NOS2 expression was similar in all myeloid cell types across WT and *Tollip*$^{-/-}$

mice (**Figure 4B**). We measured expression of MHC Class II and CD80 between Mtb-infected and uninfected myeloid cells and found that, while MHC Class II expression from each myeloid cell type was similar (data not shown), CD80 expression was significantly diminished on Mtb-infected *Tollip*$^{-/-}$ AM ($p = 0.008$), MDM ($p = 0.05$), and PMN ($p = 0.05$) four weeks post-infection (**Figure 4C**, n = 5/group) and in *Tollip*$^{-/-}$ Mtb-infected AM and MDM (**Figure 4D,** $p=0.002$ and $p=0.004$, respectively) eight weeks post-infection. In summary, NOS2 expression, a marker associated with effector function, was increased at early timepoints in Mtb-infected AM, but this was not sustained at later timepoints. In contrast, CD80 expression, a molecule critical for T cell costimulation, was diminished at both early and late timepoints in multiple Mtb-infected myeloid cell populations in *Tollip*$^{-/-}$ mice.

Intrinsic expression of TOLLIP by AM regulates immunity against Mtb. Our findings in Mtb-infected *Tollip*$^{-/-}$ mice suggested that TOLLIP expression in AM may regulate their ability to control Mtb. However, in global *Tollip*$^{-/-}$ knockout mouse models, these results could also reflect indirect effects of TOLLIP-deficiency in other cell types, or bacterial burden differences between WT and *Tollip*$^{-/-}$ mice. To directly assess the intrinsic role of TOLLIP in distinct myeloid populations, we generated mixed bone marrow chimeric mice by combining bone marrow from F1 generation *WT* mice (CD45.1+CD45.2+) in a 1:1 ratio with *Tollip*$^{-/-}$ (CD45.2+) bone marrow and transplanting this mix into CD45.1+ recipient mice (**Figure 5A**). After allowing 10 weeks for immune reconstitution and confirmation of equal proportions of immune cells from each lineage (**Figure 5B**), we infected these mice with 50-100cfu Mtb-mCherry and evaluated the induction and maintenance of the innate immune response to Mtb. Our flow gating strategy is demonstrated in **Figure S2**. We recapitulated the pattern of early innate immune responses to

Mtb (Cohen et al., 2018). 14 days after infection, AM were the primary cell infected, but increasing proportions of PMN and MDM became infected over time, as described in prior publications (**Figure 5C;** (Cohen et al., 2018). We measured the proportion of *WT* and *Tollip*$^{-/-}$ myeloid cells infected with Mtb over time. 14 days post infection, a greater percentage of *WT* AM were infected with Mtb compared with *Tollip*$^{-/-}$ AM (**Figure 5D**, p = 0.001; paired t-test, n = 5, representative of 3 independent experiments). In contrast, the percentage of Mtb-infected WT and *Tollip*$^{-/-}$ MDM and PMN were similar to each other. By d28, however, we observed a reversal of the AM phenotype; a greater percentage of *Tollip*$^{-/-}$ AM were infected compared to their WT counterparts (**Figure 5E**, p = 0.015). A modest increase in the proportion of Mtb-infected *Tollip*$^{-/-}$ PMN was also observed at d28 (**Figure 5E**, p = 0.02). Consistent with our findings in global *Tollip*$^{-/-}$ mice, we found that NOS expression was increased in *Tollip*$^{-/-}$ AM in the mixed chimeras as compared to WT AM (**Figure 5F**, p = 0.04; paired t-test; n=5). Overall, these findings show a critical AM-intrinsic role for TOLLIP in the regulation of their immune response to Mtb-infection and that the nature of this role changes over time. At early timepoints, TOLLIP deficiency in AM restricts Mtb accumulation, however, at later timepoints this is reversed and TOLLIP-deficiency in AM promotes cell-intrinsic Mtb infection.

Tollip$^{-/-}$ *AM develop ER stress gene expression signatures after Mtb infection.* The early resistance of *Tollip*$^{-/-}$ AM to Mtb infection can be explained by the observation that *Tollip*$^{-/-}$ macrophages exhibit elevated inflammatory responses and effector functions to Mtb infection, but the reason Mtb persists within AM at later timepoints is less clear. Thus, we evaluated the transcriptional networks associated with loss of Mtb control to identify alternate TOLLIP activity that alters AM function during this “post-primary” phase of infection. We sorted infected and

uninfected *Tollip*$^{-/-}$ and WT AM from mixed bone marrow chimeric mice at d28 post-infection for analysis by RNA-Seq (sorting strategy is shown in **Figure S3**). We identified 194 differentially expressed genes (DEG) between WT and *Tollip*$^{-/-}$ Mtb-infected AM (**Figure 6A**; FDR < 0.05; gene names at **Table S2**,) and 157 DEGs between WT and *Tollip*$^{-/-}$ Mtb-uninfected "bystander" AM using the same stringent FDR criteria. (**Figure 6B; Table S2**). The full gene list is available at https://github.com/altman-lab/JS20.01**.** We investigated genotype-specific gene sets in each group by applying weighted gene coexpression network analysis (WGCNA) and comparing Mtb-infected or -uninfected "bystander" AM by TOLLIP genotype. We used supervised-WGCNA, first identifying and subsetting to 3899 DEGs that met a more lenient FDR cutoff < 0.3 comparing among the 4 groups, to identify 17 distinct coexpression modules containing 54-583 genes per module (**Table S3**). The average expression of genes in each module was then modeled comparing the two AM subsets (WT vs *Tollip*$^{-/-}$) in each condition (infected or uninfected; **Figure 6C**). To understand the biological function of the genes within each module, we tested for enrichment of genes in the curated Broad Institute MSigDB Hallmark gene sets, which represent well-defined biological states and processes that display coherent expression (Liberzon et al., 2015). Multiple pathways were enriched in each module, as visualized by percent of genes in each module that map to Hallmark terms significant for at least one model (FDR < 0.05; **Figure 6D, Table S4**). Inflammatory/immune pathways (IFNγ response, TNFα signaling via NF-kB, inflammatory response, and IL2/STAT5 signaling) were enriched in modules with decreased expression in *Tollip*$^{-/-}$ AM, consistent with the prior observation that TOLLIP increases inflammation due to post-translational trafficking of immune receptors. Thus, decreased transcript here is consistent with transcriptional feedback loops to this activity and expected, based on experimental data regarding TOLLIP's mechanism of action

(Burns et al., 2000). By contrast, the unfolded protein response (ER stress response), adipogenesis, mTORC1 signaling, oxidative phosphorylation, and fatty acid metabolism were enriched in modules with increased expression in *Tollip*$^{-/-}$ AM.

To summarize the functional interpretations of RNA sequencing results, we merged modules into 6 subgroups according to a specific pattern of either significantly increased or decreased expression in *Tollip*$^{-/-}$ vs WT AM from 1) Mtb-infected AM only, 2) Mtb-uninfected bystander AM only, or 3) both Mtb-infected and -uninfected populations. We similarly evaluated for pathway enrichment in Hallmark gene sets. The modules showing increased gene expression in *Tollip*$^{-/-}$ Mtb-infected cells were significantly enriched with oxidative phosphorylation (FDR q = 3.96×10^{-56}), adipogenesis (q = 2.46×10^{-13}), MTORC1 signaling (q = 1.95×10^{-10}), fatty acid metabolism (q = 2.52×10^{-7}), and unfolded protein response (q = 9.33×10^{-6}; **Figure 6E**). The modules showing decreased expression from both Mtb-infected and bystander populations were significantly enriched for hypoxia (q = 1.93×10^{-11}) and glycolysis (q = 1.12×10^{-8}), mitotic spindle (q = 1.93×10^{-19}) and G2M checkpoint (q = 1.03×10^{-6}), both cell cycle transcriptional programs, and allograft rejection (q = 1.93×10^{-11}), inflammatory response (q = 1.93×10^{-11}), IL-2/STAT5 signaling (q = 1.12×10^{-8}), IFN-γ response (q = 1.12×10^{-8}; **Figure 6F**), which are consistent with multiple immune and inflammatory signaling pathways. The other groups did not demonstrate any significant enrichment for Hallmark gene sets. We performed Ingenuity Causal Network Analysis on genes enriched in Mtb-infected AM (FDR q < 0.05) to identify the upstream regulatory pathways responsible for the observed effects in Mtb-infected *Tollip*$^{-/-}$ AM. We found that the strongest association with increased EIF2 Signaling pathway (**Figure 6G**; z-score 2.714, p = 2.71×10^{-9}), indicative of increased cellular stress gene networks as the primary responsible pathway for phenotypes observed in **Figure 6E**, among Mtb-infected AM.

Lipid accumulation in TOLLIP-deficient macrophages induces intracellular Mtb replication.

Bioinformatic analysis suggests that EIF2 signaling, a master switch for the cellular stress response, is the upstream pathway with the strongest association with *Tollip*$^{-/-}$ Mtb-infected AM during chronic Mtb infection. Given the observation of increased foam cells in *Tollip*$^{-/-}$ mice after Mtb infection, we hypothesized that macrophages lacking TOLLIP accumulated excess lipid, which induced ER stress and maladaptive responses to Mtb. During lipid excess, autophagy and proteosomal activity are induced to control lipid droplet (LD) accumulation (Ouimet et al., 2011). TOLLIP influences ER function via endocytic transport and autophagy. We first tested the capacity of *Tollip*$^{-/-}$ macrophages to perform bulk macroautophagy. We assessed macroautophagy in bone marrow derived macrophages (BMDMs) of WT or *Tollip*$^{-/-}$ mice by measuring protein levels of LC3II and p62. To evaluate flux through autophagy, we treated BMDMs with the vATPase inhibitor Bafilomycin A (BafA), which prevents autophagosome/lysosome fusion. As expected, levels of the autophagosome protein marker LC3II were significantly upregulated following BafA treatment. Notably, *Tollip* deletion did not significantly affect levels of LC3II, nor the induction of LC3II by BafA treatment (**Figures 7A-B**). We also assessed levels of the adaptor protein p62, which both targets cargo to autophagosomes for clearance and is itself cleared during autophagy. We again observed similar levels of p62 in both groups, without significant differences in the rise of p62 following BafA treatment (**Figures 7B-C**). However, we did note a non-significant trend towards increased BafA-induced p62 accumulation in *Tollip*$^{-/-}$ cells that could reflect compensation for Tollip deficiency given analogous roles for the proteins (Lu et al., 2014; Shah et al., 2019). Nonetheless, these studies indicate that TOLLIP is dispensable for macroautophagy and

autophagic flux in macrophages. We also evaluated the impact of TOLLIP on selective autophagy of Mtb within macrophages. We infected TOLLIP-deficient and control macrophage cell lines, regularly used in our lab (Shah et al., 2016), with Mtb expressing mCherry and found no differences between these groups in the proportion of Mtb colocalizing to LC3+ autophagosomes (**Figure S4**).

We then evaluated the capacity for TOLLIP to promote lipid clearance overall. We incubated WT and *Tollip*$^{-/-}$ PEM with the mycobacterial cell wall product mycolic acid (MA; 10mg/ml) for 72 hours, stained with fluorescent dye against neutral lipid, and measured the number of LD per cell by microscopy. *Tollip*$^{-/-}$ PEM displayed significantly increased numbers of LD/cell (**Figure 7D**). We noted no difference in the proportion of PEM with quantifiable LD, indicating equal lipid uptake between cells (**Figure 7E**), but a significant increase in the number of LD in *Tollip*$^{-/-}$ PEM (**Figure 7F**, $p = 0.02$). Next, we evaluated if lung macrophages demonstrated this effect as well. We stained single cell suspensions from the lungs of mixed bone marrow chimeric mice at d28 post-infection for neutral lipid, using gating described in **Figure 6**. We found that *Tollip*$^{-/-}$ AM accumulated significantly more lipid *in vivo* than WT AM, irrespective of their infection with Mtb, while MDM did not significantly accumulate intracellular lipid (**Figure 7G**, $p = 0.03$; $n = 5$). A representative histogram for lipid accumulation in AM and MDM is displayed (**Figure 7H**; WT AM – *blue*; *Tollip*$^{-/-}$ AM – *red*).

We measured the impact of lipid accumulation on intracellular Mtb replication. We infected WT and *Tollip*$^{-/-}$ PEM with a luminescent strain of Mtb H37Rv (MOI 1; gift of Jeffrey Cox), incubated with or without MA, BSA-conjugated palmitic acid (PA-BSA), a common saturated fatty acid, or BSA-conjugated peptidoglycan (PG-BSA) as a non-lipid control. *Tollip*$^{-/-}$ PEM incubated with MA (**Figure 7I**, $p = 0.02$) or PA-BSA (**Figure 7J**, $p = 0.04$; 3-way

ANOVA accounting for TOLLIP and MA) demonstrated increased Mtb replication compared with *Tollip*$^{-/-}$ PEM in the absence of excess lipid, or WT PEM incubated with lipid. No such differences were noted after incubation with PG-BSA (**Figure 7K).** Taken together, these results show that TOLLIP prevents lipid accumulation within AM, promoting ER stress, and that dysregulation of the ER stress response in the absence of TOLLIP during chronic infection generates foamy macrophages and promotes intracellular Mtb persistence and replication.

Discussion

Genetic variants in the *TOLLIP* gene region are associated with increased risk for pulmonary and meningeal TB, but the mechanisms responsible for this phenotype are not well understood. Here we showed that mice lacking *Tollip* develop worse Mtb disease after infection, and their macrophages display a unique phenotype consistent with a dual mechanism of action -- *Tollip*$^{-/-}$ AM induce increased antimicrobial activity with improved control early in Mtb infection, but nonetheless Mtb preferentially resided within these cells after prolonged Mtb infection, when cell-cell interaction and bacterial burden are controlled. Importantly, *Tollip*$^{-/-}$ AM and PEM accumulated lipid during periods of mycobacterial persistence *in vitro* and *in vivo*. Thus, TOLLIP prevents lipid accumulation during Mtb infection, which resolves ER stress and permits ongoing Mtb control within macrophages during the chronic, “post-primary” phase of infection.

Tollip$^{-/-}$ AM accumulate lipid during Mtb infection, preventing the resolution of cellular stress. Prior studies demonstrated that TOLLIP resolves stress in endothelial cells by trafficking protein aggregates to the autophagosome (Lu et al., 2014; Pokatayev et al., 2020). Lipid

accumulation induces ER stress (Volmer et al., 2013), which has multiple downstream effects observed in *Tollip*$^{-/-}$ AM after chronic Mtb infection, including abnormal lipid metabolism, maladaptive energetics, and cell cycle arrest. However, the pathways responsible for lipid clearance and control of ER stress remain unknown. Excess lipids are cleared from cells via lipolysis followed by proteosomal secretion, or by autophagic recycling (lipophagy; (Finn and Dice, 2006; Singh et al., 2009; Zhang and Wang, 2016)). During periods of normal lipid flux, lipolysis and cholesterol secretion are sufficient to maintain ER homeostasis. By contrast, lipophagy is activated to transport LD to lysosomes for recycling and export during episodes of lipid excess (Ouimet et al., 2011). TOLLIP participates in both autophagy (Lu et al., 2014) and endosomal cargo transport (Jongsma et al., 2016). Therefore, understanding how TOLLIP influences autophagic or proteosomal export and degradation of lipids may determine future therapeutic strategies to resolve lipid-induced cellular stress. Moreover, the TOLLIP protein domains responsible for preventing lipid accumulation are undefined. TOLLIP contains four conserved protein domains: a Tom1 binding domain, a C2 phospholipid binding domain, two autophagosome interacting motifs (AIM), and a ubiquitin binding CUE domain (Burns et al., 2000; Chen et al., 2017; Xiao et al., 2015). The AIM and CUE domains are both required for autophagic clearance of protein aggregates, (Lu et al., 2014) and the CUE domain is essential for ER cargo transport through its E3 ubiquitin ligase RNF26 (Jongsma et al., 2016). However, individuals with mutations in Tom1 that impair TOLLIP binding develop lung disease and immunodeficiency, suggesting an important functional role for the TBD as well (Keskitalo et al., 2019). Understanding the specific domains from TOLLIP required for lipid metabolism and cell signaling in the context of Mtb infection may provide strategies for selective lipid lowering or immune regulation.

Multiple lines of evidence suggest that lipid accumulation is important for Mtb pathogenesis, but several hypotheses remain to explain the specific impacts on host-pathogen interactions. Macrophages accumulate lipid bodies after Mtb infection (Knight et al., 2018; Ouimet et al., 2016; Russell et al., 2009). These intracellular changes in lipid flux are accompanied by alterations in host cell energy utilization (Singh et al., 2012). Furthermore, lipid accumulation is associated with permissive Mtb replication and impaired innate immune responses. Granuloma cores are lipid-rich, forming “caseum” which is associated with increased Mtb growth (Kim et al., 2010). However, the effects of Mtb-induced lipid accumulation on macrophage function remain incompletely understood. Mtb may utilize host lipids as an energy source. Mtb can survive on lipids alone in liquid culture, and Mtb accumulates lipids derived from host macrophages (Lee et al., 2013). Triglyceride accumulation in macrophages induces a dormant state in Mtb (Daniel et al., 2011; Marrero et al., 2010). However, direct evidence of this phenomenon remains undefined. Alternately, LDs form in response to IFNγ, and LD formation is programmed by IFNγ after infection to enhance eicosanoid infection (Knight et al., 2018). LD may then act as sources for proinflammatory eicosanoids to enhance Mtb killing. However, lipid accumulation is maladaptive overall during Mtb infection. Our data suggests an alternate role as storage for excess host and bacterial fatty acids to prevent cellular stress and toxicity while awaiting recycling or export. Accumulated LD may then contribute to TB pathogenesis directly via trehalose dimycolate to induce further stress and toxicity (Hunter et al., 2006). Regardless of mechanisms, selectively preventing intracellular lipid accumulation in AM may improve Mtb outcomes by sensitizing this reservoir for Mtb to immune signals.

How excess fatty acid permits Mtb replication within macrophages is not known. Fatty acids induce cellular toxicity after destabilizing lysosomal membranes and increasing their permeability (Almaguel et al., 2010) and depleting calcium within the ER, which leads to mitochondrial oxidative stress (Xu et al., 2015). In settings of lysosomal permeability, cathepsins and other components of toxic granules may cross into the cytoplasm and induce macrophage necrosis and further exacerbate cellular stress. (Ferri and Kroemer, 2001; Kagedal et al., 2001). Recent zebrafish studies demonstrate that ER calcium flux and reactive oxygen species determine Mtb-induced macrophage cell death and Mtb escape from the macrophage (Roca et al., 2019). Acid sphingomyelinase, a lysosomal enzyme, is required to cleave ceramide to sphingosine, which specifically induces lysosomal permeability (Roca and Ramakrishnan, 2013). In Mtb-infected *Tollip*$^{-/-}$ AM, we note strong enrichment of sphingolipid metabolic pathways. Combined with the observation that TOLLIP prevents lipid accumulation, we surmise that TOLLIP-deficient macrophages accumulate excess sphingosine to create lysosomal permeability and permit Mtb replication.

In mixed bone marrow chimera experiments, *Tollip*$^{-/-}$ AM developed increased Mtb burden 28 days post-infection. However, full knockout mice developed increased bacterial burden eight weeks post-infection. The reason for this observed difference is uncertain. Chimeric mice undergo full body radiation and bone marrow transplant, and this disruption of the bone marrow impacts future immune responses, including influencing the immune response to pathogens. Decreased TOLLIP expression is associated with impaired lung transplant engraftment, and so TOLLIP deficiency may selectively influence the immune response to mycobacteria after bone marrow reconstitution (Cantu et al., 2016). However, we identified these

phenotypes within multiple mouse models, and find this phenotype recapitulated in genetic studies of TOLLIP (Shah et al., 2016; Shah et al., 2012). Alternately, intracellular carriage of mycobacteria within AM may more sensitively measure mycobacterial burden than total lung Mtb bacterial CFU, as intracellular replication within AM may precede replication in the lung overall. Thus, our observations in AMs using mixed bone marrow chimeric mice may represent a "leading indicator" toward the chronic, maladaptive phenotype.

We focused on the impact of TOLLIP on macrophage biology in this study and discovered that it plays an AM-intrinsic role in lipid clearance, but TOLLIP is ubiquitously expressed and may influence the function of multiple immune cell subsets. Selective autophagy receptors alter dendritic cell function, particularly during EBV, influenza, yellow fever vaccine, and *L. monocytogenes* infection (Lee et al., 2010; Ravindran et al., 2014; Schmid et al., 2007). ER stress response protein XBP1 prevents dendritic cell apoptosis and permits T cell activation during lipid excess in ovarian cancer models (Kaser et al., 2008). TOLLIP may also impact T cell activation and differentiation. Another selective autophagy receptor, TAX1BP1, permits T cells to meet the energy demands of activation and proliferation (Whang et al., 2017), and autophagy supports regulatory T cell lineage stability by maintaining its metabolic homeostasis (Wei et al., 2016). Thus, TOLLIP may influence autophagy and cellular homeostasis across immune cell types during the immune response.

Studies from the preantibiotic era regularly describe "post-primary" tuberculosis as an obstructive lipoid pneumonia, but its impact on Mtb pathogenesis is not clearly defined (Hunter, 2016). In these studies, the pathologic and radiographic sign of progressive post-primary TB is

not the cavitating granuloma, but rather acute, paucibacillary, caseating lipoid pneumonia obstructing bronchioles in a “tree-in-bud” pattern (Cornil and Ranvier, 1880; Hunter, 2011; Im et al., 1995). Macrophages develop foamy appearance within these obstructed alveoli, leading to subsequent lipoid necrosis and granuloma formation around this caseum. This obstructive lipoid pneumonia precedes the transition from asymptomatic to symptomatic TB disease (Hunter, 2016). The absence of a clear animal model equivalent for this phenomenon, and waning interest this phenotype with the development of antimycobacterial therapy led to poor understanding of this stage of Mtb pathogenesis (Hunter, 2016). However, these data suggest multiple immune or cellular checkpoints for Mtb progression. We find that intracellular accumulation of lipid, due to impairment from TOLLIP deficiency, is an independent risk factor for TB progression at a time point equivalent to “post-primary” TB. These data offer a plausible mechanism for Mtb progression during this intermediate phase of infection by inducing AM to develop foamy phenotypes and inducing lipid-dependent maladaptive cellular stress responses. We found that lipid-laden, stressed AM infected with Mtb undergo cell cycle arrest and impaired metabolic adaptation to Mtb infection, which provided a replicative niche for Mtb despite increasing inflammation in the surrounding tissues. Thus, a combination of genetic factors that influence lipid clearance and physical factors that obstruct ciliary clearance of lipid debris, may set the stage for progressive TB disease. Providing means to 1) promote ongoing lipid clearance or 2) relieve bronchial obstruction during the earliest phases of Mtb infection may prevent TB progression from early silent infection to symptomatic disease. Further, therapies to prevent this phenotype or resolve it may sensitize macrophages to immune signals, improving the effectiveness of vaccine candidates.

TOLLIP diminishes TLR and NOS2 responses *in vivo* and simultaneously clears excess intracellular lipid after Mtb infection. Recent studies demonstrate a balance between TOLLIP's role in resolving ER stress from overexpression of the Huntingtin protein and maintaining STING expression and activity (Pokatayev et al., 2020). Together, these data demonstrate that TOLLIP links macrophage homeostasis through lipid clearance with regulating innate immune responses. Obesity and metabolic syndrome, diseases of increased lipid and glucose characterized by dysregulated homeostasis, are associated epidemiologically to multiple infectious diseases, including TB and viral respiratory infections, but the molecular mechanisms underlying how these disease influence immune pathogenesis are poorly understood (Falagas and Kompoti, 2006). TOLLIP may balance maintaining homeostasis from excess lipid with orchestrating immune responses to Mtb. Understanding how cells maintain homeostasis may provide novel therapeutic approaches for both metabolic syndrome and TB. We demonstrate that TOLLIP is necessary to maintain macrophage effectiveness during prolonged Mtb infection. Moreover, TOLLIP is required to balance lipid flux and innate immune responses in the lung and influences cellular homeostasis by preventing intracellular lipid accumulation. In the absence of these phenotypes, Mtb-infected AMs demonstrate permissive replication and increased ER stress. Preventing lipid accumulation via TOLLIP may be an effective host directed therapeutic strategy.

Acknowledgements

The authors wish to thank the University of Washington Center for Lung Biology Histology and Imaging Core for their helpful advice on pathology staining and analysis. We are grateful to the Seattle Children's Research Institute Cell Sorting Core for their assistance and technical support.

This work was supported by the NIH(R01 AI136912 to JAS; R01 DK108921 to SAS) and the Department of Veterans Affairs (I01 BX004444 to SAS). GLP was supported by the American Diabetes Association (19-PDF-063).

Author Contributions

Conceptualization: SV, KU, SS JS; methodology: SV, SS, KU, MA, JS; software: KDM, MA; validation: SV, JS, RE; formal analysis: MA, KDM; investigation: SV, CP, GP, AL, AP, RP, JS; writing – original draft: SV, JS; writing – review and editing: KU, SS, MA, CP; supervision: JS, KU, MA, SS; project administration: SV, JS; funding acquisition: JS, KU, SS, MA.

Declaration of Interests

The authors declare no competing interests.

Figure Legends

Figure 1. TOLLIP deficiency induces a proinflammatory cytokine bias in Mtb-infected macrophages. Peritoneal exudate macrophages (PEM) were isolated, plated in tissue culture, and stimulated with LPS (10 ng/ml), PAM3 (250 ng/ml), and Mtb whole cell lysate (1mcg/ml) overnight. Cell culture supernatants (mean ± SD) were obtained and **A)** TNF and **B)** IL-10 concentrations were measured by ELISA. PEM were infected with Mtb H37Rv (MOI 2.5) overnight, then cell culture supernatants were collected and **C)** TNF, **D)** IL-1β and **E)** IL-10 were measured by ELISA (mean ± SD). Two-sided t-test was used to determine statistical significance between groups. N=3/group, experiment was performed three times independently.

Figure 2. TOLLIP is required for Mtb control in mice and its absence induces foam cell formation. Mice were infected with Mtb H37Rv (50-100 cfu) via aerosol and monitored over time. **A)** Experimental timeline. **B-C)** Lung bacterial burden in WT (*clear circle*) and *Tollip*$^{-/-}$ (*black square*) mice **B)** 1-2 weeks and **C**) 4 weeks and later after infection. Spleen bacterial burden **D**) 1-2 weeks and **E)** 4 weeks and later after infection. * $p < 0.05$; ** $p < 0.01$, ***$p < 0.001$, two-sided t-test at each time point; n = 5 mice/group. Overall associations were determined using a two-sided ANOVA accounting for time and genotype. **F)** Survival curve analysis of WT (*clear circle*) and *Tollip*$^{-/-}$ (*black square*) mice after aerosol infection with 50-100cfu Mtb H37Rv strain. N = 10 mice/group. $P < 0.0001$, Mantel-Cox test. **G)** Percentage of initial body weight after Mtb aerosol infection *Circle* – WT mice; *square* - *Tollip*$^{-/-}$ mice. N = 10 / group. **H)** Hematoxylin and eosin staining of Mtb-infected lung tissue from WT and *Tollip*$^{-/-}$ mice 4 and 8 weeks after aerosol infection. **I)** Experimental outline of full bone marrow chimera experiments. **J)** Lung bacterial burden of bone marrow chimeric mice, 8 weeks after aerosol Mtb infection. N = 5 mice/group. * $p < 0.05$, ** $p < 0.01$, *** $p < 0.001$.

Figure 3. Mtb preferentially infects *Tollip*-deficient myeloid cells 8 weeks after aerosol infection. Lungs from Mtb-infected mice were gently dissociated, and flow cytometry was performed. Gating strategy described in **Supplemental Figure 1**. The proportion of lung resident myeloid cells from WT (*clear circle*) and *Tollip*$^{-/-}$ (*black square*) mice was compared **A)** 4 and **B)** 8 weeks after aerosol infection with 50-100 cfu mCherry-expressing Mtb. The proportion of each cell subset infected with Mtb (mCherry+) was compared between groups **C)** 4 and **D)** 8 weeks post infection. N = 5 mice/group. Experiment was performed three times independently. Statistical significance determined using Student's t-test. AM – alveolar

macrophage, MDM – monocyte-derived macrophage, IM – interstitial macrophage, PMN – neutrophil, DC – dendritic cell.

Figure 4. *Tollip*$^{-/-}$ lung-resident myeloid cells develop enhanced antimicrobial responses after Mtb infection. Please see **Supplemental Figure 1** for gating strategy to identify myeloid cell subsets. **A and B)** Intracellular NOS2 protein expression was measured in Mtb-infected lung-resident myeloid cells (mCherry+) by flow cytometry **A)** 4 and **B)** 8 weeks post infection. CD80 expression was measured **C)** 4 and **D)** 8 weeks post infection. Median fluorescence intensity was compared using a two-sided t-test. N = 5 mice/group. WT (*clear circle*); *Tollip*$^{-/-}$ (*black square*). Experiment was repeated three times independently. AM – alveolar macrophage, MDM – monocyte-derived macrophage, IM – interstitial macrophage, PMN – neutrophil, DC – dendritic cell.

Figure 5. *Tollip*$^{-/-}$ lung resident myeloid cells become preferentially infected with Mtb over time. WT:*Tollip*$^{-/-}$ mixed bone marrow chimeric mice were infected with Mtb expressing mCherry (50-100 cfu) and followed. Gating strategy can be found in **Figure S2**. **A)** Experimental strategy and timeline. Mixed bone marrow chimeras were generated by mixing 1:1 ratios of WT (CD45.1+/CD45.2+) and *Tollip*$^{-/-}$ (CD45.2+) mice and transferred to a CD45.1+ murine host. **B)** Frequency distribution of CD45 expression in naïve mixed bone marrow chimeric mice. **C)** Composition of mCherry+ lung leukocytes at the indicated time point. **D and E)** Distribution of mCherry+ cells at **D)** d14 and **E)** d28 post-infection in mixed bone marrow chimeric mice. **F)** Median fluorescence intensity of nitric oxide synthase (NOS) in AM at d28 post-infection from

mixed bone marrow chimeric mice. N = 4 or 5 mice for each time point as indicated; experiments were conducted three times independently. * $p < 0.05$, ** $p < 0.005$. Significance determined by paired two-sided t-test. AM – alveolar macrophage, MDM – monocyte-derived macrophage, IM – interstitial macrophage, PMN – neutrophil.

Figure 6. Global gene expression analysis of Mtb-infected *Tollip*$^{-/-}$ AM demonstrates increased cell stress. Mixed bone marrow chimeric mice were infected with mCherry-expressing Mtb and 28 days after infection, Mtb-infected and Mtb-uninfected WT and *Tollip*$^{-/-}$ AM were sorted and RNA-seq was performed. Sorting strategy can be found in **Figure S3**. **A)** Volcano plot of gene expression (log2 fold change) and significance (-log10(FDR)) for genes between *Tollip*$^{-/-}$ (CD45.2) and WT (CD45.1+CD45.2+), Mtb-uninfected and **B)** Mtb-infected AMs. Horizontal lines indicate significant genes (FDR < 0.05) and genes used in WGCNA modules (FDR < 0.3) **C)** Heatmap of mean module z-score for infection: TOLLIP groups. Red bars indicate increased expression in *Tollip*$^{-/-}$ AM and blue bars indicated decreased expression in *Tollip*$^{-/-}$ AM, separated by infection status. Modules (columns) were average hierarchical clustered. **D)** Heat map of enrichment of significant Hallmark gene sets (FDR q-value < 0.05) in modules. Color indicates percent of genes in a module that mapped to a given Hallmark. The total number of genes in each module is indicated above. Modules (columns) were clustered as in **C)** and Hallmark terms (rows) were average hierarchical clustered based on enrichment percentages. Red and blue bars are as in **C)**. **E-F)** Bar graph of the Hallmark terms enriched in modules with **E)** increased expression in Mtb-infected, *Tollip*$^{-/-}$AM or **F)** decreased expression in both Mtb-infected and bystander AM. Bar length indicates the proportional enrichment of each

pathway. Color indicates degree of significance: *purple* – FDR $q < 10^{-16}$; *red* -- $q < 10^{-8}$; *orange* – $q < 10^{-4}$. **G)** Ingenuity Pathway Analysis of upstream regulatory pathways enriched by data for Mtb-infected cells. *Orange* bar indicates increased expression in *Tollip*$^{-/-}$ AM. *Gray* bars indicate no directional data available.

Figure 7. *Tollip*$^{-/-}$ macrophages accumulate excess lipid that creates a permissive environment for Mtb replication. Bone marrow from WT (*black bars*) or *Tollip*$^{-/-}$ (*white bars*) were differentiated *ex vivo* to macrophages using 40ng/mL mCSF for 7-9 days. Following differentiation, BMDMs were treated for 6hr with or without 250nM Bafilomycin A (BafA). **A**) Representative western blot results showing protein levels of LC3I/II and p62. **B**) Quantification of protein levels (by densitometry) of LC3II using total LC3 (I+II) as a loading control. ***p<0.001 2-way ANOVA for an effect of BafA **C**) Quantification of p62 levels (by densitometry) using vinculin as a loading control. p=0.056 2-way ANOVA effect of BafA. **D-F**) WT and *Tollip*$^{-/-}$ peritoneal exudate macrophages (PEM) were isolated and incubated with mixed mycolic acids (MA) for 72hrs. PEM were stained with LipidTOX Red dye (*red*) and DAPI (*blue*), fixed, and visualized with fluorescent microscopy. **D)** Representative image for of lipid droplet (LD) accumulation in WT and *Tollip*$^{-/-}$ PEM. **E)** Percentage of cells with visible LD, of 100 cells imaged. Bar – error bars (mean ± SD). **F)** Total number of LD per cell, of 100 cells with detectable LD. Bar – error bars (mean ± SD). **G)** Median fluorescence intensity of alveolar macrophages (AM) and monocyte-derived macrophages (MDM) stained with LipidTox neutral lipid stain from mixed bone marrow chimeric mice 28 days after Mtb infection. Infection and gating were performed as in **Figures 5**. Lines connect WT and *Tollip*$^{-/-}$ AM from the same mouse. Significance calculated using two-sided paired t-test. **H)** Representative histogram of

AM and MDM lipid staining from one experiment (WT – blue; *Tollip*$^{-/-}$ – red). **I-K)** Luminescence over time in WT and *Tollip*$^{-/-}$ PEM's incubated with exogenous lipid - MA, mycolic acid (10µg/ml); PA, palmitic acid conjugated to BSA, (10µg/ml); PG, peptidoglycan conjugated to BSA (10µg/ml) and infected with Mtb Erdman expressing *lux* luminescence gene (MOI 1). PEMs were isolated and incubated with MA for 72 hr before infection, while PA and PG were added to culture at the time of infection. Intracellular replication was measured by luminescence for each group over the next three days in quadruplicate and repeated three times to assess reproducibility. Statistical significance was determined by 3-way ANOVA accounting for time, genotype, and lipid administration.

Experimental Procedures

A complete list of reagents can be found in **Table S1 (Key Resources Table)**. Abbreviations and description of bioinformatics tools and all bioinformatic data and code can be found at https://github.com/altman-lab/JS20.01.

Mice

B6.Cg-Tollip^{tm1Kbns}/Cnrm (*Tollip*$^{-/-}$) mice were obtained from the European Mutant Mouse Archive (www.infrafrontier.eu) (Didierlaurent et al., 2006). Mice were backcrossed 11 times on C57BL/6J background and were confirmed to be >99% C57BL/6J genetically by screening 150 SNP ancestry informative markers (Jax, Inc). Genotyping was performed using DNA primers for neomycin (Forward sequence: AGG ATC TCC TGT CAT CTC ACC TTG CTC CTG; Reverse sequence AAG AAC TCG TCA AGA AGG CGA TAG AAG GCG) and the first exon of TOLLIP (Forward sequence: AGC TAC TGG GAG GCC ATA CA; Reverse sequence: CGT

GTA CGG GAG ACC CAT TT). Protein expression was confirmed in both knockout and backcrossed alleles by qPCR and Western blot. All wild type control mice were age-matched littermates to ensure a common genetic background. All mice were housed and maintained in specific pathogen-free conditions at the University of Washington and Seattle Children's Research Institute, and all experiments were performed in compliance with the Institutional Animal Care and Use Committee from each institution. Mice used in the experiments were 6-12 weeks of age. ABSL3 experiments were performed at the Seattle Children's Global Infectious Disease Research Institute.

Chimera Generation

WT:*Tollip*$^{-/-}$ mixed bone marrow chimeras were generated in the following manner: WT B6.SJL-Ptprca Pepcb/BoyJ (CD45.1+; Jax, Inc.) F1 mice were lethally irradiated (1000 cGy). A 1:1 mixture of CD3-depleted (Miltenyi Biotec) *Tollip*$^{-/-}$ (CD45.2+) and F1 generation of C57BL/6J (CD45.1+45.2+) bone marrow was provided intravenously. For full bone marrow chimera generation, WT and *Tollip*$^{-/-}$ mice were irradiated, followed by hemopoietic reconstitution by adoptive transfer of 5-10x10^6 bone marrow cells via intravenous injection.

Model of Mtb aerosol infection

Aerosol infections were performed with wildtype H37Rv Mtb or H37Rv Mtb with an mCherry reporter plasmid (Cosma et al., 2004). Mice were enclosed in a Glas-Col aerosol infection chamber and ~50-100 CFU were deposited into mouse lungs. Doses were confirmed using control mice by plating lung homogenates on 7H10 agar immediately after aersosol infection. Mice were sacrificed at indicated timepoint, and lungs were gently homogenized in PBS-

containing 0.05%Tween using a gentleMacs dissociator (Miltenyi Biotec). Tissue homogenates were serially diluted on 7H10 agar and lung CFU was enumerated.

Tissue Preparation and Evaluation

Mice were euthanized and lungs were gently homogenized in HEPES buffer containing Liberase Blendzyme 3 (70 μg/ml; Roche) and DNaseI (30 μg/ml; Sigma-Aldrich) using a gentleMacs dissociator (Miltenyi Biotec). The lungs were then incubated for 30 min at 37°C and then further homogenized a second time with the gentleMacs. The homogenates were filtered through a 70 μm cell strainer, pelleted for RBC lysis with RBC lysing buffer (Thermo), and resuspended in FACS buffer (PBS containing 2.5% FBS and 0.1% NaN_3). To prepare organs for histology, lung sections were inflated to 15cm water pressure with 4% paraformaldehyde, fixed in the same solution, embedded in paraffin and 4μm sections were generated. Sections stained with hematoxylin and eosin were examined by a pathologist blinded to mouse genotype.

Intracellular Mtb replication assay.

Frozen Mtb was thawed and cultured on a shaking incubator for two doubling cycles. One day prior to infection, cultures were back-diluted into an optical density (OD) of 0.2–0.4 in 7H9 media supplemented with glycerol (4%), Middlebrook ADC Growth Supplement (100 mL/L), and Tween 80 (0.05%). At the time of infection, Mtb was filtered through a 5 μm syringe filter to remove bacterial clumps, and cells were inoculated at indicated MOI. The inoculum was prepared in RPMI-10 medium and applied to cells, which were centrifuged at 1200rpm for 5 minutes and incubated for 4 hours at 37°C. Supernatants were removed, and washed twice with prewarmed PBS (phosphate-buffered saline) to remove unbound bacteria, before adding per

warmed RPMI supplemented with 10% FBS. Intracellular growth was determined using luminescence on a Synergy H4 multimode microplate reader (Biotek Instruments) daily from Day 0 to Day 3. In some experiments, 24hrs post infection cell culture supernatants were collected and filtered twice using 0.22µm filter and frozen at -80°C.

Macrophage Preparation

Resident peritoneal cells, mainly consisting of *in vivo* differentiated macrophages, were isolated using standard methods (Zhang, X et al 2008). Briefly, 10ml of cold PBS was injected using 27g needle, and peritoneum was gently messaged. Cells were removed with PBS, centrifuged at 4° C and placed into warm RPMI media. PEMs (1×10^5/well) were plated in 96-well plates in 200µL of antibiotic-free RPMI 1640 containing with 10% Fetal Bovine Serum (Atlas Biologics). Cell were rested for minimum 24hrs before further experimentation. Bone marrow was harvested from mice and grown in RPMI supplemented with 10% heat inactivated FBS and M-CSF (40ng/ml) in tissue culture treated plates. Cells were then incubated at 37º C for 6 to 7 days. Bone marrow-derived macrophages (BMDM) were used after 7 days of culture. BMDMs were detached by gently scrapping and cells were then plated in RPMI 1640 supplemented with 10% heat inactivated FBS.

Lung Cell Flow Cytometry

Lung single cell suspensions were washed and stained for viability with Zombie Aqua viability dye (BioLegend) for 10 min at room temperature in the dark. After incubation, 100 µl of a surface antibody cocktail diluted in 50% FACS buffer/50% 24G2 Fc block buffer was added and surface staining was performed for 30 min at 4°C. Antibody lists can be found in **Table S1**. The

cells were washed once with FACS buffer and fixed with 2% paraformaldehyde for 1 h prior to analyzing on an LSRII flow cytometer (BD Biosciences). In some experiments, intracellular staining was performed after surface staining. Permeabilization was peformed with Fix-Perm buffer (eBiosciences) for minimum of 60 min before the addition of intracellular antibodies. Then cells were fixed with 2% paraformaldehyde for 1 h prior to analyzing on an LSRII flow cytometer (BD Biosciences). For cell sorting, mice were infected with Mtb H37Rv expressing mCherry (gift of David Sherman). 28 days after infection, mice were sacrificed, and AM were sorted on a BD FACSAria in a BSL-3 facility for infected and uninfected populations**.** The samples were spun and stored -80° C in Trizol.

Cellular Studies

Cell-culture supernatants were collected at indicated time and frozen at -20 □C until analysis. The cytokine concentrations in the culture supernatant were determined using quantitative ELISA (Mouse TNF and IL-10 DuoSet; R&D Systems) as recommended by the manufacturer. For detection of lipid bodies, PEMs from WT and *Tollip*$^{-/-}$ mice were plated (1×10^5/well) in a glass bottom chamber slide. Lipid was added as previously described (Peyron et al., 2008). Cells were washed twice and resuspended in PBS solution of HCS LipidTOX Deep Red Neutral Lipid stain (ThermoFisher Scientific) according to manufacturer instruction. After incubation, cells were washed twice with PBS and fixed in 2% PFA for 30min. Cells were mounted in medium containing DAPI stain (ProLong Gold, Thermo, Inc.). Lipid droplets were counted from 100 cells identified randomly selected high-powered fields.

Western blotting

Immunoblots were performed as described previously (Soleimanpour et al., 2014). Briefly, 5-20µg of cell or tissue protein extract was separated by SDS-PAGE, transferred onto PVDF membranes and immunoblotted with primary antibodies, listed in **Table S1**. Secondary antibodies conjugated to horseradish peroxidase were added and luminescence was quantitated.

Preparation of total RNA and sequencing

Total RNA from sorted cells was isolated using the manufacturer's instructions (TRIzol, Invitrogen). The RNA purity and quantified was assessed by RNA-Tapestation (Agilent 4200). cDNA was prepared using SMART-Seq v4 Ultra Low Input RNA Kit (Takara Bio USA, Inc). RNA sequencing libraries were prepared using the Illumina TruSeq™ RNA Sample Preparation Kit (Illumina, San Diego, CA, USA). Samples were sequenced as 50 bp paired-end reads on a Illumina HiSeq 2500 and assessed using FastQC v0.11.8 to visualize sequence quality (Andrews, 2010). Sequences were filtered using AdapterRemoval v2.3.1 to remove adapters, remove sequences with >1 ambiguous base, and trim ends to a 30+ Phred score (Schubert et al., 2016). Sequences were aligned to the mouse genome mm10 using STAR v2.7.4a (Dobin et al., 2013), and alignments were assessed with Picard v2.18.7 (2019) and samtools v1.10 (Li et al., 2009). Total reads in gene exons were quantified using featureCounts v2.0.1 (Liao et al., 2013).

Differential expression analysis

Gene expression analyses were performed in R v3.6.1 with the tidyverse v1.3.0 (Wickham et al., 2019). Overall, samples were very high-quality with > 32 million aligned sequences per sample and low variability in gene coverage (median coefficient of variation coverage < 0.6). Genes were filtered to protein coding genes with biomaRt (N = 21850) with > 0.1 counts per million

(CPM) in at least three samples (N = 14215) (Durinck et al., 2005). Counts were normalized for RNA composition using edgeR and log2 CPM voom normalized with quality weights using limma (Ritchie et al., 2015; Robinson et al., 2010). Differentially expressed genes were determined using limma using a contrasts model comparing WT and *Tollip*$^{-/-}$ cells in uninfected and infected groups (**Table S2**). Genes with FDR < 0.3 for at least one contrast (N = 3899) were clustered into modules using WCGNA (Langfelder and Horvath, 2008) with a minimum R-squared of 0.8 and minimum module size of 50. This resulted in 17 modules, leaving out 282 genes not grouped into any module (**Table S3**). Module expression was calculated as the mean expression of the log2 values of the genes within each module and assessed for differential expression using the same contrasts model in limma. Modules were functionally assessed using clusterProfiler v3.12.0 to compare them to the Broad Institute Hallmark gene sets in msigbr v7.0.1 by hypergeometric distribution (Dolgalev, 2019; Yu et al., 2012). The Benjamini–Hochberg correction for multiple comparisons was applied to P-values and significance was assessed at FDR < 0.05 for all tests.

Supplemental Information

Table S1. Key Resources Table.

Table S2. List of differentially expressed genes (DEG) in Mtb- infected and Mtb-uninfected *Tollip*$^{-/-}$ AM compared to WT AM from the same mice.

Table S3. List of genes in each WGCNA module comparing sorted WT and *Tollip*$^{-/-}$ AM.

Table S4. List of GSEA hallmark pathways significantly enriched in each WGCNA module comparing sorted WT and *Tollip*$^{-/-}$ AM.

References

(2019). Picard Toolkit. (Broad Institute).

Almaguel, F.G., Liu, J.W., Pacheco, F.J., De Leon, D., Casiano, C.A., and De Leon, M. (2010). Lipotoxicity-mediated cell dysfunction and death involve lysosomal membrane permeabilization and cathepsin L activity. Brain Res *1318*, 133-143.

Andrews, S. (2010). FastQC: A Quality Control Tool for High Throughput Sequence Data.

Burns, K., Clatworthy, J., Martin, L., Martinon, F., Plumpton, C., Maschera, B., Lewis, A., Ray, K., Tschopp, J., and Volpe, F. (2000). Tollip, a new component of the IL-1RI pathway, links IRAK to the IL-1 receptor. Nat Cell Biol *2*, 346-351.

Cantu, E., Suzuki, Y., Diamond, J.M., Ellis, J., Tiwari, J., Beduhn, B., Nellen, J.R., Shah, R., Meyer, N.J., Lederer, D.J., *et al.* (2016). Protein Quantitative Trait Loci Analysis Identifies Genetic Variation in the Innate Immune Regulator TOLLIP in Post-Lung Transplant Primary Graft Dysfunction Risk. Am J Transplant *16*, 833-840.

Chen, K., Yuan, R., Geng, S., Zhang, Y., Ran, T., Kowalski, E., Liu, J., and Li, L. (2017). Toll-interacting protein deficiency promotes neurodegeneration via impeding autophagy completion in high-fat diet-fed ApoE-/- mouse model. Brain Behav Immun *59*, 200-210.

Cohen, S.B., Gern, B.H., Delahaye, J.L., Adams, K.N., Plumlee, C.R., Winkler, J.K., Sherman, D.R., Gerner, M.Y., and Urdahl, K.B. (2018). Alveolar Macrophages Provide an Early Mycobacterium tuberculosis Niche and Initiate Dissemination. Cell Host Microbe *24*, 439-446 e434.

Consortium, G.T. (2015). Human genomics. The Genotype-Tissue Expression (GTEx) pilot analysis: multitissue gene regulation in humans. Science *348*, 648-660.

Cornil, V., and Ranvier, L. (1880). A manual of pathological histology translated with notes and additions by EO Shakespeare and JHC Simms. Philadephia: Henry C Lea, 394-445.

Daniel, J., Maamar, H., Deb, C., Sirakova, T.D., and Kolattukudy, P.E. (2011). Mycobacterium tuberculosis uses host triacylglycerol to accumulate lipid droplets and acquires a dormancy-like phenotype in lipid-loaded macrophages. PLoS Pathog *7*, e1002093.

Didierlaurent, A., Brissoni, B., Velin, D., Aebi, N., Tardivel, A., Kaslin, E., Sirard, J.C., Angelov, G., Tschopp, J., and Burns, K. (2006). Tollip regulates proinflammatory responses to interleukin-1 and lipopolysaccharide. Mol Cell Biol *26*, 735-742.

Dobin, A., Davis, C.A., Schlesinger, F., Drenkow, J., Zaleski, C., Jha, S., Batut, P., Chaisson, M., and Gingeras, T.R. (2013). STAR: ultrafast universal RNA-seq aligner. Bioinformatics (Oxford, England) *29*, 15-21.

Dolgalev, I. (2019). msigdbr: MSigDB Gene Sets for Multiple Organisms in a Tidy Data Format.

Durinck, S., Moreau, Y., Kasprzyk, A., Davis, S., De Moor, B., Brazma, A., and Huber, W. (2005). BioMart and Bioconductor: a powerful link between biological databases and microarray data analysis. Bioinformatics *21*, 3439-3440.

Falagas, M.E., and Kompoti, M. (2006). Obesity and infection. Lancet Infect Dis *6*, 438-446.

Ferri, K.F., and Kroemer, G. (2001). Organelle-specific initiation of cell death pathways. Nat Cell Biol *3*, E255-263.

Finn, P.F., and Dice, J.F. (2006). Proteolytic and lipolytic responses to starvation. Nutrition *22*, 830-844.

Grootjans, J., Kaser, A., Kaufman, R.J., and Blumberg, R.S. (2016). The unfolded protein response in immunity and inflammation. Nat Rev Immunol *16*, 469-484.

Guilliams, M., De Kleer, I., Henri, S., Post, S., Vanhoutte, L., De Prijck, S., Deswarte, K., Malissen, B., Hammad, H., and Lambrecht, B.N. (2013). Alveolar macrophages develop from fetal monocytes that differentiate into long-lived cells in the first week of life via GM-CSF. J Exp Med *210*, 1977-1992.

Gutierrez, M.G., Master, S.S., Singh, S.B., Taylor, G.A., Colombo, M.I., and Deretic, V. (2004). Autophagy is a defense mechanism inhibiting BCG and Mycobacterium tuberculosis survival in infected macrophages. Cell *119*, 753-766.

Hunter, R.L. (2011). Pathology of post primary tuberculosis of the lung: an illustrated critical review. Tuberculosis (Edinb) *91*, 497-509.

Hunter, R.L. (2016). Tuberculosis as a three-act play: A new paradigm for the pathogenesis of pulmonary tuberculosis. Tuberculosis (Edinb) *97*, 8-17.

Hunter, R.L., Olsen, M., Jagannath, C., and Actor, J.K. (2006). Trehalose 6,6'-dimycolate and lipid in the pathogenesis of caseating granulomas of tuberculosis in mice. In Am J Pathol, pp. 1249-1261.

Im, J.G., Itoh, H., Lee, K.S., and Han, M.C. (1995). CT-pathology correlation of pulmonary tuberculosis. Crit Rev Diagn Imaging *36*, 227-285.

Jongsma, M.L., Berlin, I., Wijdeven, R.H., Janssen, L., Janssen, G.M., Garstka, M.A., Janssen, H., Mensink, M., van Veelen, P.A., Spaapen, R.M., and Neefjes, J. (2016). An ER-Associated Pathway Defines Endosomal Architecture for Controlled Cargo Transport. Cell *166*, 152-166.

Kagedal, K., Johansson, U., and Ollinger, K. (2001). The lysosomal protease cathepsin D mediates apoptosis induced by oxidative stress. FASEB J *15*, 1592-1594.

Kaser, A., Lee, A.H., Franke, A., Glickman, J.N., Zeissig, S., Tilg, H., Nieuwenhuis, E.E., Higgins, D.E., Schreiber, S., Glimcher, L.H., and Blumberg, R.S. (2008). XBP1 links ER stress

to intestinal inflammation and confers genetic risk for human inflammatory bowel disease. Cell *134*, 743-756.

Keskitalo, S., Haapaniemi, E.M., Glumoff, V., Liu, X., Lehtinen, V., Fogarty, C., Rajala, H., Chiang, S.C., Mustjoki, S., Kovanen, P., *et al.* (2019). Dominant TOM1 mutation associated with combined immunodeficiency and autoimmune disease. NPJ Genom Med *4*, 14.

Kim, M.J., Wainwright, H.C., Locketz, M., Bekker, L.G., Walther, G.B., Dittrich, C., Visser, A., Wang, W., Hsu, F.F., Wiehart, U., *et al.* (2010). Caseation of human tuberculosis granulomas correlates with elevated host lipid metabolism. EMBO Mol Med *2*, 258-274.

Kimmey, J.M., Huynh, J.P., Weiss, L.A., Park, S., Kambal, A., Debnath, J., Virgin, H.W., and Stallings, C.L. (2015). Unique role for ATG5 in neutrophil-mediated immunopathology during M. tuberculosis infection. Nature *528*, 565-569.

Knight, M., Braverman, J., Asfaha, K., Gronert, K., and Stanley, S. (2018). Lipid droplet formation in Mycobacterium tuberculosis infected macrophages requires IFN-gamma/HIF-1alpha signaling and supports host defense. PLoS Pathog *14*, e1006874.

Langfelder, P., and Horvath, S. (2008). WGCNA: an R package for weighted correlation network analysis. BMC Bioinformatics *9*, 559.

Lee, H.K., Mattei, L.M., Steinberg, B.E., Alberts, P., Lee, Y.H., Chervonsky, A., Mizushima, N., Grinstein, S., and Iwasaki, A. (2010). In vivo requirement for Atg5 in antigen presentation by dendritic cells. Immunity *32*, 227-239.

Lee, W., VanderVen, B.C., Fahey, R.J., and Russell, D.G. (2013). Intracellular Mycobacterium tuberculosis exploits host-derived fatty acids to limit metabolic stress. J Biol Chem *288*, 6788-6800.

Levine, B., Mizushima, N., and Virgin, H.W. (2011). Autophagy in immunity and inflammation. Nature *469*, 323-335.

Li, H., Handsaker, B., Wysoker, A., Fennell, T., Ruan, J., Homer, N., Marth, G., Abecasis, G., Durbin, R., and Subgroup, G.P.D.P. (2009). The Sequence Alignment/Map format and SAMtools. Bioinformatics (Oxford, England) *25*, 2078-2079.

Liao, Y., Smyth, G.K., and Shi, W. (2013). featureCounts: an efficient general purpose program for assigning sequence reads to genomic features. Bioinformatics *30*, 923-930.

Liberzon, A., Birger, C., Thorvaldsdottir, H., Ghandi, M., Mesirov, J.P., and Tamayo, P. (2015). The Molecular Signatures Database (MSigDB) hallmark gene set collection. Cell Syst *1*, 417-425.

Lu, K., Psakhye, I., and Jentsch, S. (2014). Autophagic clearance of polyQ proteins mediated by ubiquitin-Atg8 adaptors of the conserved CUET protein family. Cell *158*, 549-563.

Marrero, J., Rhee, K.Y., Schnappinger, D., Pethe, K., and Ehrt, S. (2010). Gluconeogenic carbon flow of tricarboxylic acid cycle intermediates is critical for Mycobacterium tuberculosis to establish and maintain infection. Proc Natl Acad Sci U S A *107*, 9819-9824.

Matsuzawa-Ishimoto, Y., Hwang, S., and Cadwell, K. (2018). Autophagy and Inflammation. Annu Rev Immunol *36*, 73-101.

Mizushima, N., and Komatsu, M. (2011). Autophagy: renovation of cells and tissues. Cell *147*, 728-741.

Oh, J., Riek, A.E., Weng, S., Petty, M., Kim, D., Colonna, M., Cella, M., and Bernal-Mizrachi, C. (2012). Endoplasmic reticulum stress controls M2 macrophage differentiation and foam cell formation. J Biol Chem *287*, 11629-11641.

Ouimet, M., Franklin, V., Mak, E., Liao, X., Tabas, I., and Marcel, Y.L. (2011). Autophagy regulates cholesterol efflux from macrophage foam cells via lysosomal acid lipase. Cell Metab *13*, 655-667.

Ouimet, M., Koster, S., Sakowski, E., Ramkhelawon, B., van Solingen, C., Oldebeken, S., Karunakaran, D., Portal-Celhay, C., Sheedy, F.J., Ray, T.D., *et al.* (2016). Mycobacterium tuberculosis induces the miR-33 locus to reprogram autophagy and host lipid metabolism. Nat Immunol *17*, 677-686.

Peyron, P., Vaubourgeix, J., Poquet, Y., Levillain, F., Botanch, C., Bardou, F., Daffe, M., Emile, J.F., Marchou, B., Cardona, P.J., *et al.* (2008). Foamy macrophages from tuberculous patients' granulomas constitute a nutrient-rich reservoir for M. tuberculosis persistence. PLoS Pathog *4*, e1000204.

Pokatayev, V., Yang, K., Tu, X., Dobbs, N., Wu, J., Kalb, R.G., and Yan, N. (2020). Homeostatic regulation of STING protein at the resting state by stabilizer TOLLIP. Nat Immunol *21*, 158-167.

Ravindran, R., Khan, N., Nakaya, H.I., Li, S., Loebbermann, J., Maddur, M.S., Park, Y., Jones, D.P., Chappert, P., Davoust, J., *et al.* (2014). Vaccine activation of the nutrient sensor GCN2 in dendritic cells enhances antigen presentation. Science *343*, 313-317.

Ritchie, M.E., Phipson, B., Wu, D., Hu, Y., Law, C.W., Shi, W., and Smyth, G.K. (2015). limma powers differential expression analyses for RNA-sequencing and microarray studies. Nucleic acids research *43*, e47-e47.

Robinson, M.D., McCarthy, D.J., and Smyth, G.K. (2010). edgeR: a Bioconductor package for differential expression analysis of digital gene expression data. Bioinformatics (Oxford, England) *26*, 139-140.

Roca, F.J., and Ramakrishnan, L. (2013). TNF dually mediates resistance and susceptibility to mycobacteria via mitochondrial reactive oxygen species. Cell *153*, 521-534.

Roca, F.J., Whitworth, L.J., Redmond, S., Jones, A.A., and Ramakrishnan, L. (2019). TNF Induces Pathogenic Programmed Macrophage Necrosis in Tuberculosis through a Mitochondrial-Lysosomal-Endoplasmic Reticulum Circuit. Cell *178*, 1344-1361 e1311.

Russell, D.G., Cardona, P.J., Kim, M.J., Allain, S., and Altare, F. (2009). Foamy macrophages and the progression of the human tuberculosis granuloma. Nat Immunol *10*, 943-948.

Russell, D.G., Huang, L., and VanderVen, B.C. (2019). Immunometabolism at the interface between macrophages and pathogens. Nat Rev Immunol *19*, 291-304.

Schmid, D., Pypaert, M., and Munz, C. (2007). Antigen-loading compartments for major histocompatibility complex class II molecules continuously receive input from autophagosomes. Immunity *26*, 79-92.

Schubert, M., Lindgreen, S., and Orlando, L. (2016). AdapterRemoval v2: rapid adapter trimming, identification, and read merging. BMC research notes *9*, 88-88.

Shah, J.A., Berrington, W.R., Vary, J.C., Jr., Wells, R.D., Peterson, G.J., Kunwar, C.B., Khadge, S., Hagge, D.A., and Hawn, T.R. (2016). Genetic Variation in Toll-Interacting Protein Is Associated With Leprosy Susceptibility and Cutaneous Expression of Interleukin 1 Receptor Antagonist. J Infect Dis *213*, 1189-1197.

Shah, J.A., Emery, R., Lee, B., Venkatasubramanian, S., Simmons, J.D., Brown, M., Hung, C.F., Prins, J.M., Verbon, A., Hawn, T.R., and Skerrett, S.J. (2019). TOLLIP deficiency is associated with increased resistance to Legionella pneumophila pneumonia. Mucosal Immunol *12*, 1382-1390.

Shah, J.A., Musvosvi, M., Shey, M., Horne, D.J., Wells, R.D., Peterson, G.J., Cox, J.S., Daya, M., Hoal, E.G., Lin, L., *et al.* (2017). A Functional TOLLIP Variant is Associated with BCG-Specific Immune Responses and Tuberculosis. Am J Respir Crit Care Med.

Shah, J.A., Vary, J.C., Chau, T.T., Bang, N.D., Yen, N.T., Farrar, J.J., Dunstan, S.J., and Hawn, T.R. (2012). Human TOLLIP Regulates TLR2 and TLR4 Signaling and Its Polymorphisms Are Associated with Susceptibility to Tuberculosis. J Immunol *189*, 1737-1746.

Singh, R., Kaushik, S., Wang, Y., Xiang, Y., Novak, I., Komatsu, M., Tanaka, K., Cuervo, A.M., and Czaja, M.J. (2009). Autophagy regulates lipid metabolism. Nature *458*, 1131-1135.

Singh, V., Jamwal, S., Jain, R., Verma, P., Gokhale, R., and Rao, K.V. (2012). Mycobacterium tuberculosis-driven targeted recalibration of macrophage lipid homeostasis promotes the foamy phenotype. Cell Host Microbe *12*, 669-681.

Soleimanpour, S.A., Gupta, A., Bakay, M., Ferrari, A.M., Groff, D.N., Fadista, J., Spruce, L.A., Kushner, J.A., Groop, L., Seeholzer, S.H., *et al.* (2014). The diabetes susceptibility gene Clec16a regulates mitophagy. Cell *157*, 1577-1590.

Volmer, R., van der Ploeg, K., and Ron, D. (2013). Membrane lipid saturation activates endoplasmic reticulum unfolded protein response transducers through their transmembrane domains. Proc Natl Acad Sci U S A *110*, 4628-4633.

Wei, J., Long, L., Yang, K., Guy, C., Shrestha, S., Chen, Z., Wu, C., Vogel, P., Neale, G., Green, D.R., and Chi, H. (2016). Autophagy enforces functional integrity of regulatory T cells by coupling environmental cues and metabolic homeostasis. Nat Immunol *17*, 277-285.

Whang, M.I., Tavares, R.M., Benjamin, D.I., Kattah, M.G., Advincula, R., Nomura, D.K., Debnath, J., Malynn, B.A., and Ma, A. (2017). The Ubiquitin Binding Protein TAX1BP1

Mediates Autophagasome Induction and the Metabolic Transition of Activated T Cells. Immunity *46*, 405-420.

Wickham, H., Averick, M., Bryan, J., Chang, W., McGowan, L.D.A., François, R., Grolemund, G., Hayes, A., Henry, L., Hester, J., *et al.* (2019). Welcome to the Tidyverse. Journal of Open Source Software *4*, 1686-1686.

Xiao, S., Brannon, M.K., Zhao, X., Fread, K.I., Ellena, J.F., Bushweller, J.H., Finkielstein, C.V., Armstrong, G.S., and Capelluto, D.G.S. (2015). Tom1 Modulates Binding of Tollip to Phosphatidylinositol 3-Phosphate via a Coupled Folding and Binding Mechanism. Structure *23*, 1910-1920.

Xu, S., Nam, S.M., Kim, J.H., Das, R., Choi, S.K., Nguyen, T.T., Quan, X., Choi, S.J., Chung, C.H., Lee, E.Y., *et al.* (2015). Palmitate induces ER calcium depletion and apoptosis in mouse podocytes subsequent to mitochondrial oxidative stress. Cell Death Dis *6*, e1976.

Yu, G., Wang, L.-G., Han, Y., and He, Q.-Y. (2012). clusterProfiler: an R package for comparing biological themes among gene clusters. Omics : a journal of integrative biology *16*, 284-287.

Zhang, L., and Wang, H.H. (2016). The essential functions of endoplasmic reticulum chaperones in hepatic lipid metabolism. Dig Liver Dis *48*, 709-716.

Figure 1

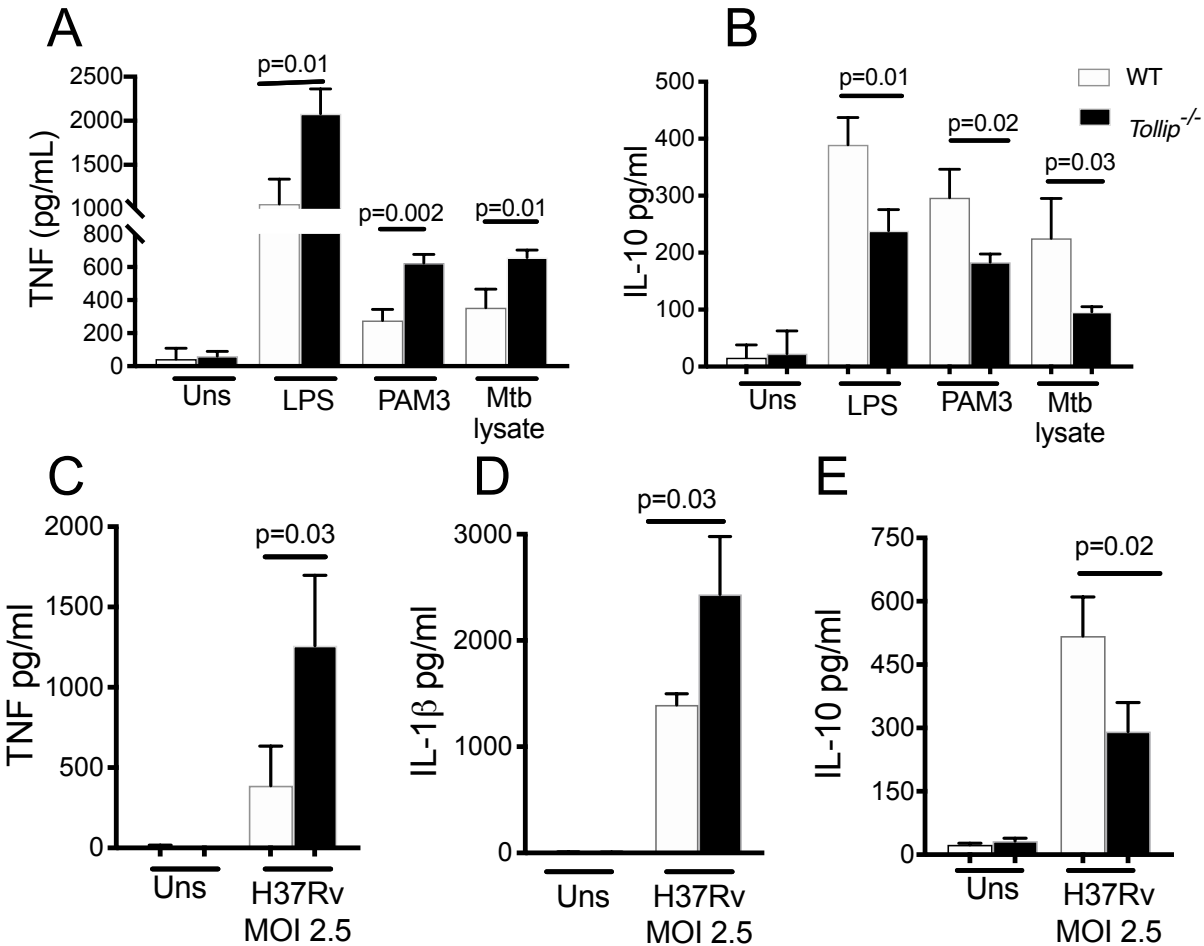
A
TNF (pg/mL)
2500
2000
1500
1000
800
600
400
200
0
p=0.01
p=0.002
p=0.01
Uns
LPS
PAM3
Mtb lysate
B
IL-10 pg/ml
500
400
300
200
100
0
p=0.01
p=0.02
p=0.03
WT
Tollip-/-
Uns
LPS
PAM3
Mtb lysate
C
TNF pg/ml
2000
1500
1000
500
0
p=0.03
Uns
H37Rv MOI 2.5
D
IL-1β pg/ml
3000
2000
1000
0
p=0.03
Uns
H37Rv MOI 2.5
E
IL-10 pg/ml
750
600
450
300
150
0
p=0.02
Uns
H37Rv MOI 2.5

Figure 2

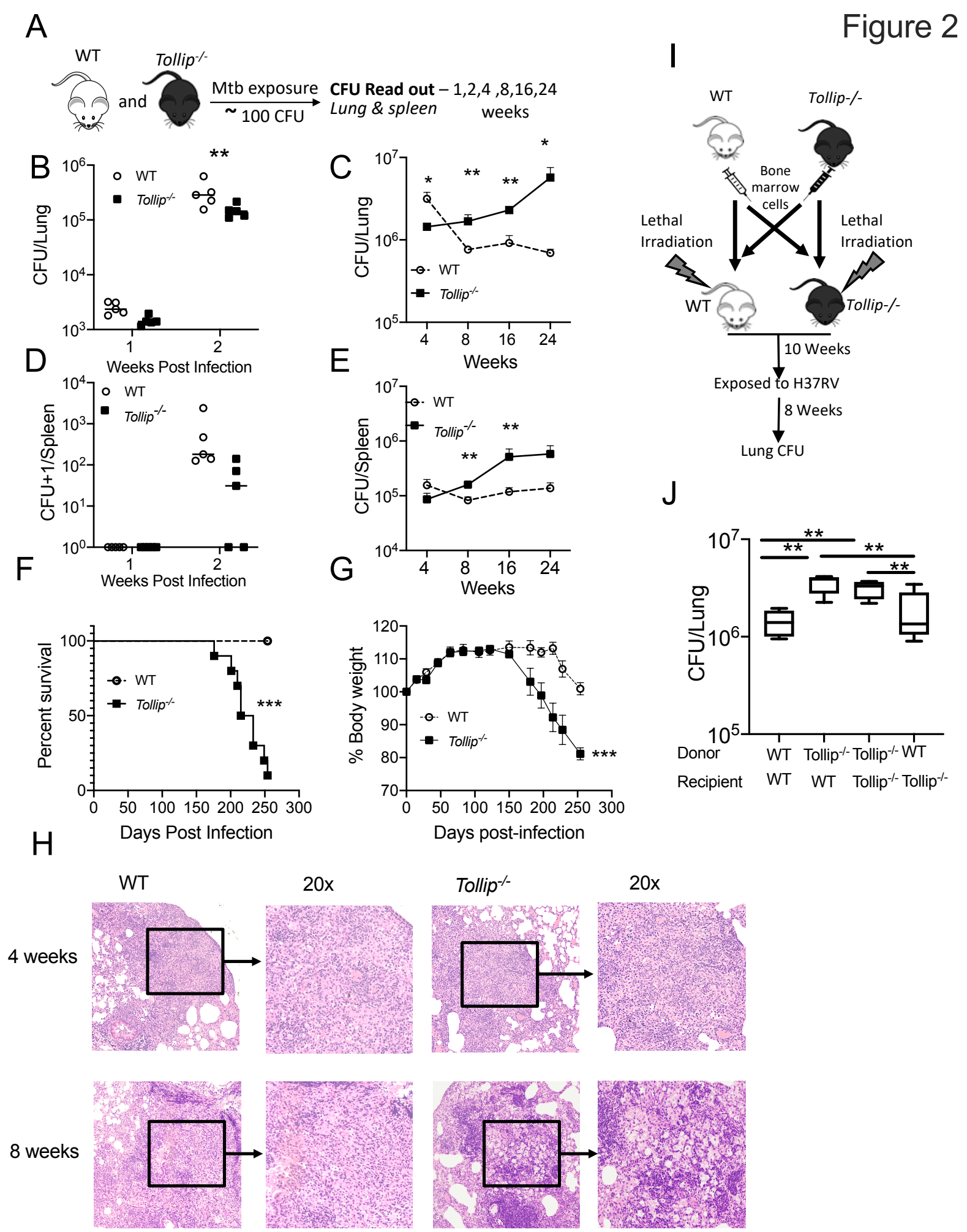
A
WT
Tollip-/-
and
Mtb exposure
~ 100 CFU
CFU Read out – 1,2,4 ,8,16,24 weeks
Lung & spleen
B
CFU/Lung
Weeks Post Infection
C
CFU/Lung
Weeks
D
CFU+1/Spleen
Weeks Post Infection
E
CFU/Spleen
Weeks
F
Percent survival
Days Post Infection
G
% Body weight
Days post-infection
I
Bone marrow cells
Lethal Irradiation
10 Weeks
Exposed to H37RV
8 Weeks
Lung CFU
J
CFU/Lung
Donor
Recipient
H
20x
4 weeks
8 weeks

Figure 3

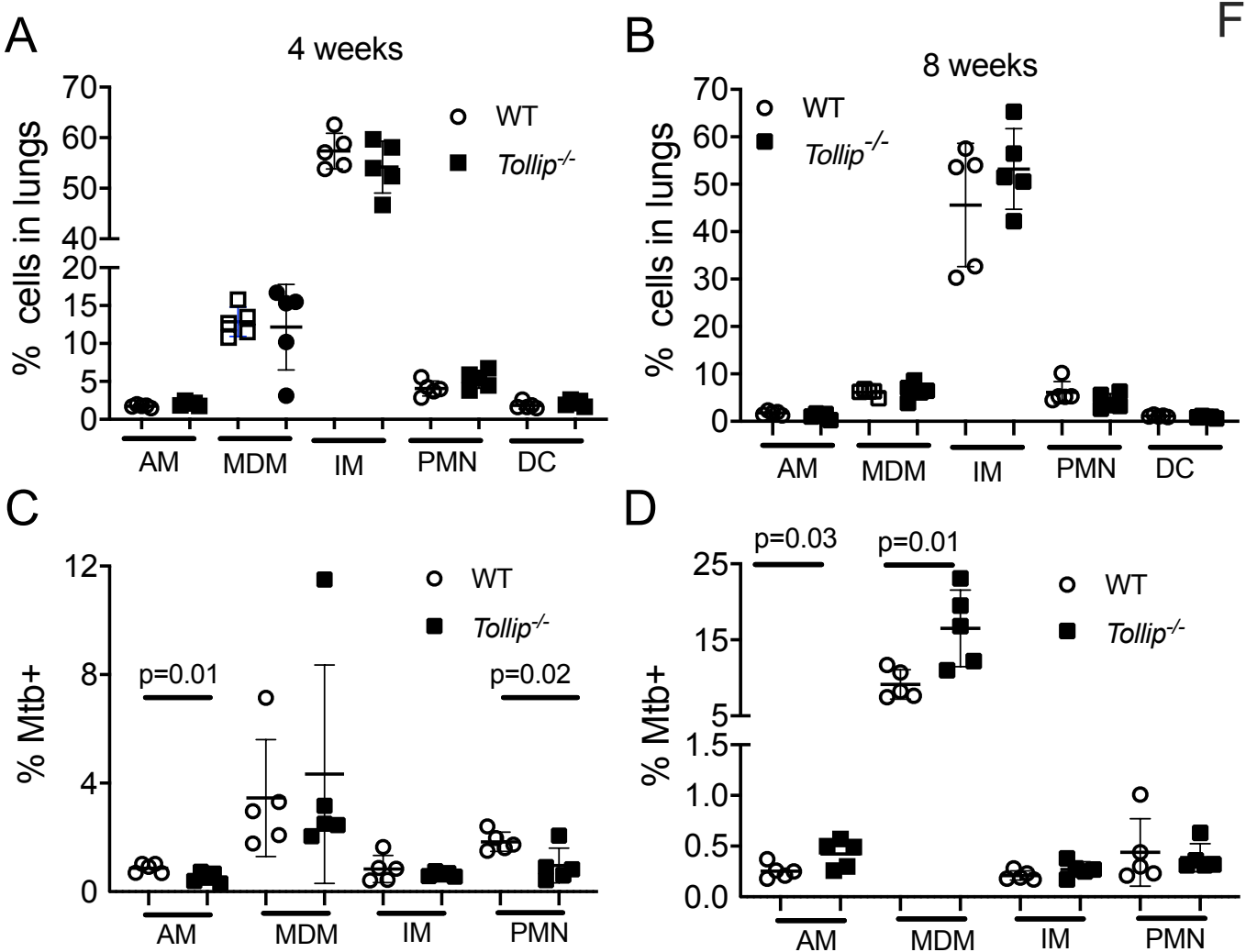
A
4 weeks
% cells in lungs
WT
Tollip-/-
AM
MDM
IM
PMN
DC
B
8 weeks
% cells in lungs
WT
Tollip-/-
AM
MDM
IM
PMN
DC
C
% Mtb+
p=0.01
p=0.02
WT
Tollip-/-
AM
MDM
IM
PMN
D
% Mtb+
p=0.03
p=0.01
WT
Tollip-/-
AM
MDM
IM
PMN

Figure 4

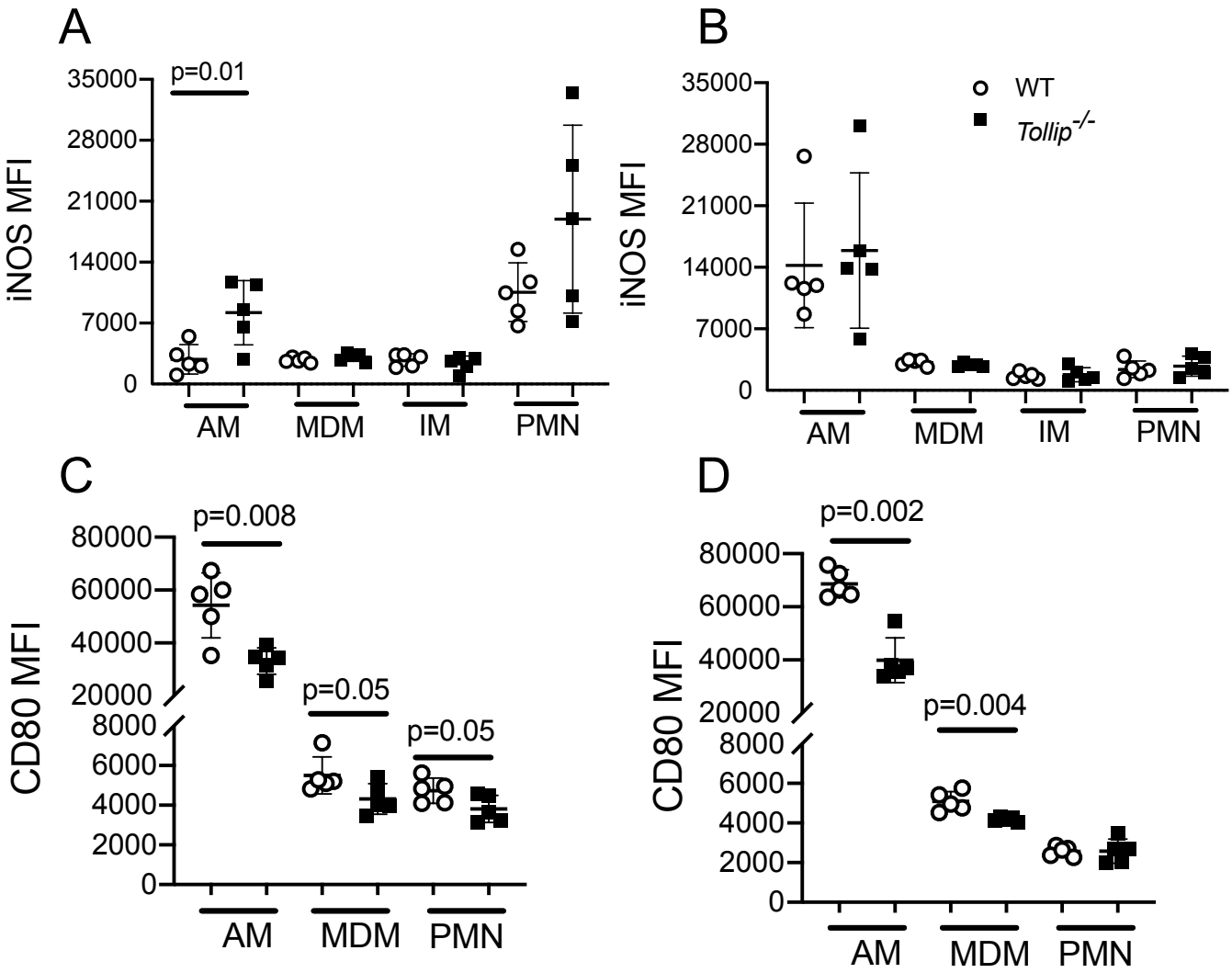
A
p=0.01
35000
28000
21000
14000
7000
0
iNOS MFI
AM
MDM
IM
PMN
B
WT
Tollip-/-
35000
28000
21000
14000
7000
0
iNOS MFI
AM
MDM
IM
PMN
C
p=0.008
80000
60000
40000
20000
p=0.05
p=0.05
8000
6000
4000
2000
0
CD80 MFI
AM
MDM
PMN
D
p=0.002
80000
60000
40000
20000
p=0.004
8000
6000
4000
2000
0
CD80 MFI
AM
MDM
PMN

Figure 5

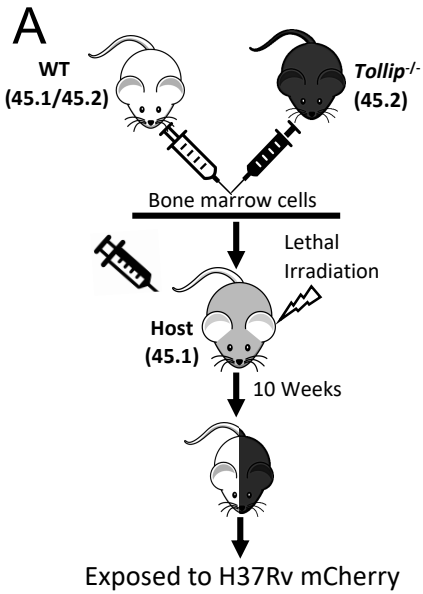
A
WT
(45.1/45.2)
Tollip-/-
(45.2)
Bone marrow cells
Lethal
Irradiation
Host
(45.1)
10 Weeks
Exposed to H37Rv mCherry

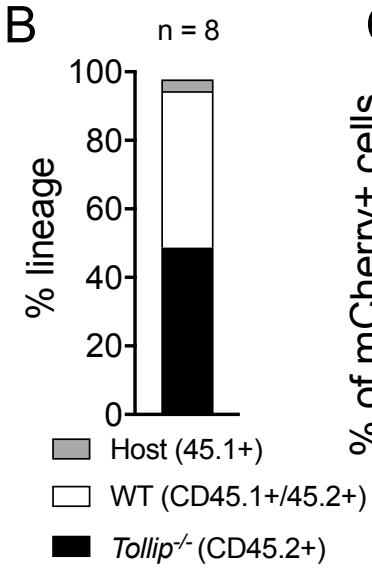
B
n = 8
% lineage
100
80
60
40
20
0
Host (45.1+)
WT (CD45.1+/45.2+)
Tollip-/- (CD45.2+)

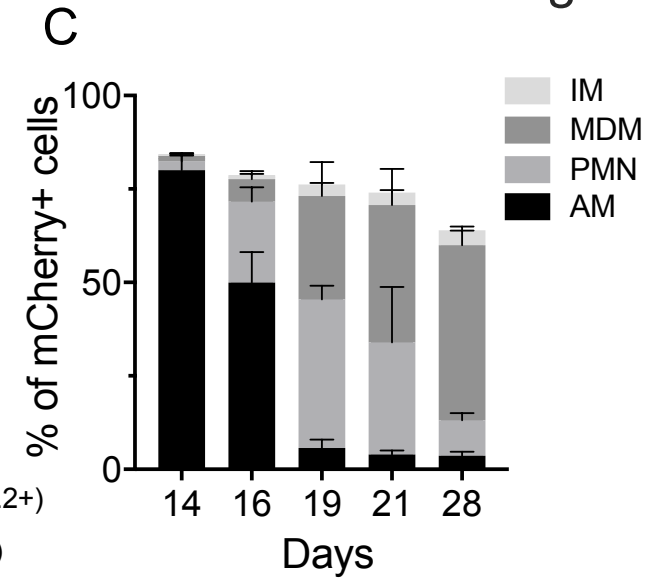
C
% of mCherry+ cells
100
50
0
IM
MDM
PMN
AM
14
16
19
21
28
Days

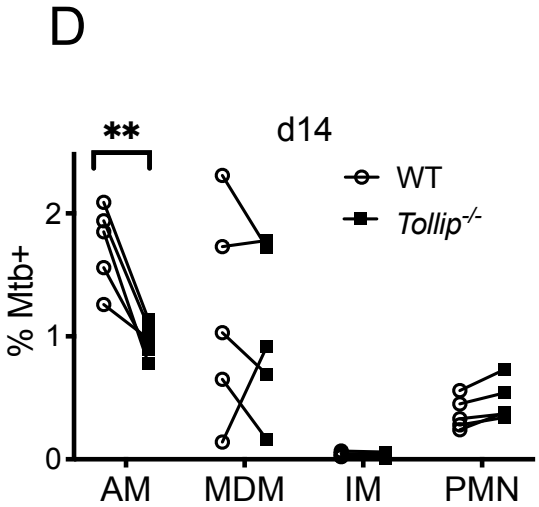
D
d14
**
% Mtb+
2
1
0
WT
Tollip-/-
AM
MDM
IM
PMN

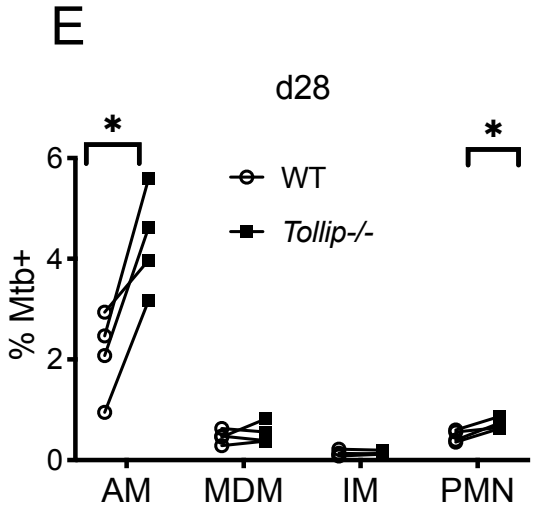
E
d28
*
*
% Mtb+
6
4
2
0
WT
Tollip-/-
AM
MDM
IM
PMN

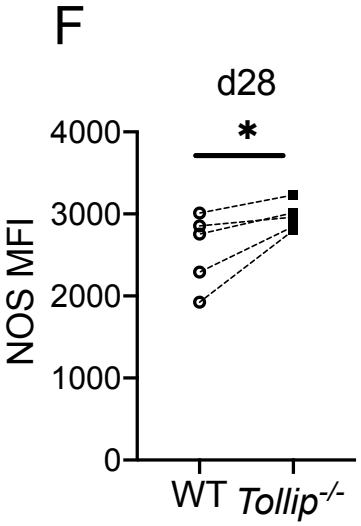
F
d28
*
NOS MFI
4000
3000
2000
1000
0
WT
Tollip-/-

Figure 6

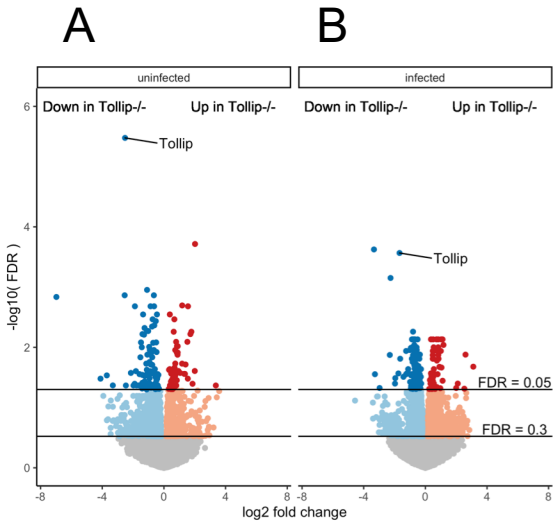
A
B
uninfected
infected
Down in Tollip-/-
Up in Tollip-/-
Tollip
FDR = 0.05
FDR = 0.3
-log10(FDR)
log2 fold change

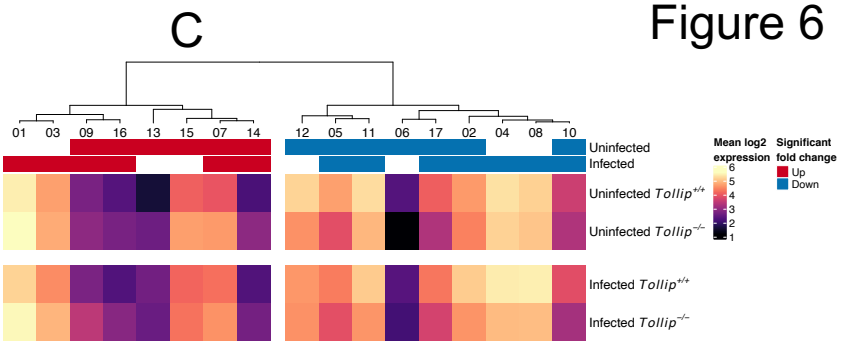
C
01 03 09 16 13 15 07 14
12 05 11 06 17 02 04 08 10
Uninfected
Infected
Uninfected Tollip+/+
Uninfected Tollip−/−
Infected Tollip+/+
Infected Tollip−/−
Mean log2 expression
Significant fold change
Up
Down

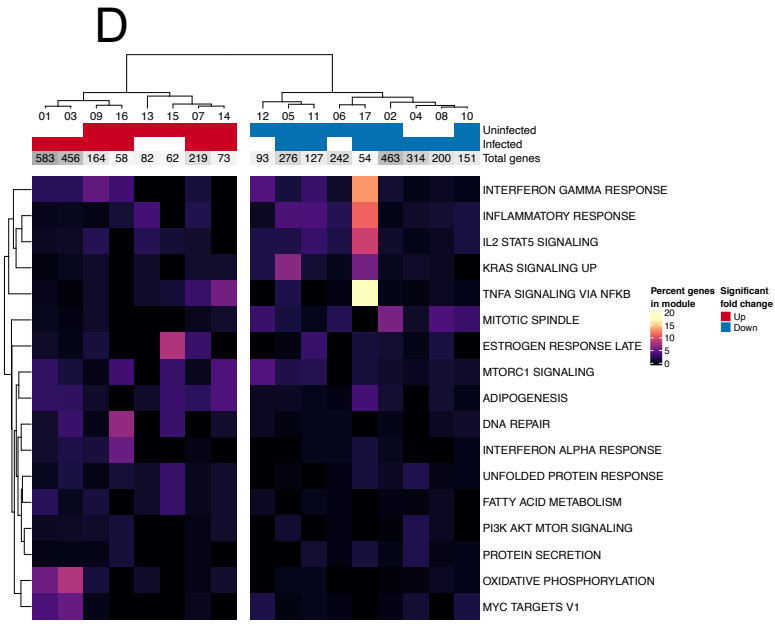
D
01 03 09 16 13 15 07 14
12 05 11 06 17 02 04 08 10
Uninfected
Infected
583 456 164 58 82 62 219 73
93 276 127 242 54 463 314 200 151
Total genes
INTERFERON GAMMA RESPONSE
INFLAMMATORY RESPONSE
IL2 STAT5 SIGNALING
KRAS SIGNALING UP
TNFA SIGNALING VIA NFKB
MITOTIC SPINDLE
ESTROGEN RESPONSE LATE
MTORC1 SIGNALING
ADIPOGENESIS
DNA REPAIR
INTERFERON ALPHA RESPONSE
UNFOLDED PROTEIN RESPONSE
FATTY ACID METABOLISM
PI3K AKT MTOR SIGNALING
PROTEIN SECRETION
OXIDATIVE PHOSPHORYLATION
MYC TARGETS V1
Percent genes in module
Significant fold change
Up
Down

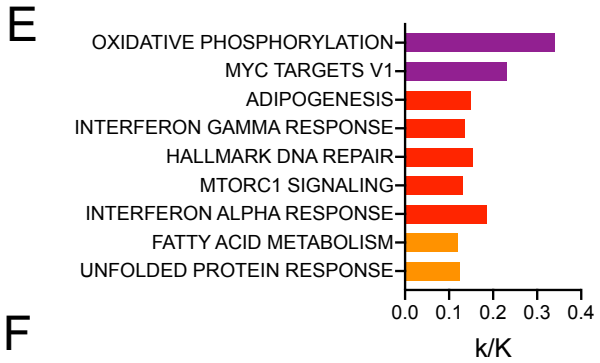
E
OXIDATIVE PHOSPHORYLATION
MYC TARGETS V1
ADIPOGENESIS
INTERFERON GAMMA RESPONSE
HALLMARK DNA REPAIR
MTORC1 SIGNALING
INTERFERON ALPHA RESPONSE
FATTY ACID METABOLISM
UNFOLDED PROTEIN RESPONSE
0.0 0.1 0.2 0.3 0.4
k/K

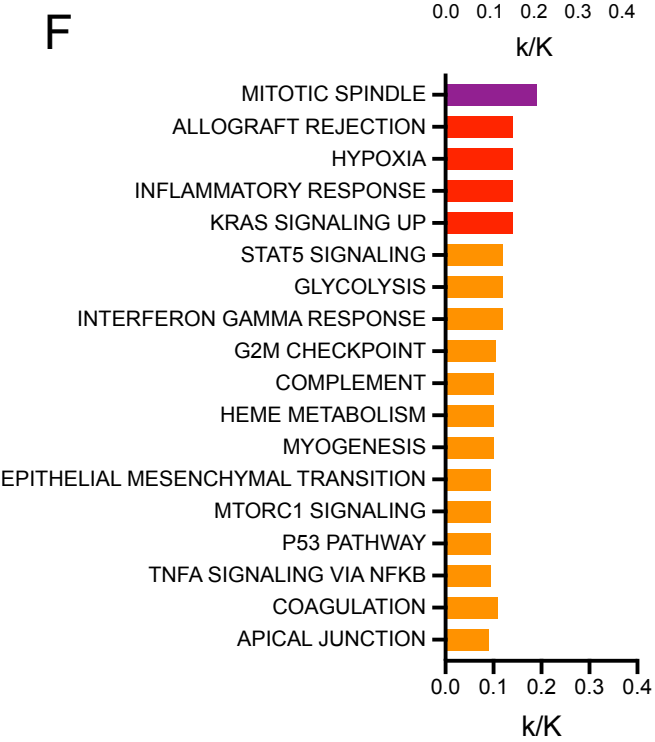
F
MITOTIC SPINDLE
ALLOGRAFT REJECTION
HYPOXIA
INFLAMMATORY RESPONSE
KRAS SIGNALING UP
STAT5 SIGNALING
GLYCOLYSIS
INTERFERON GAMMA RESPONSE
G2M CHECKPOINT
COMPLEMENT
HEME METABOLISM
MYOGENESIS
EPITHELIAL MESENCHYMAL TRANSITION
MTORC1 SIGNALING
P53 PATHWAY
TNFA SIGNALING VIA NFKB
COAGULATION
APICAL JUNCTION
0.0 0.1 0.2 0.3 0.4
k/K

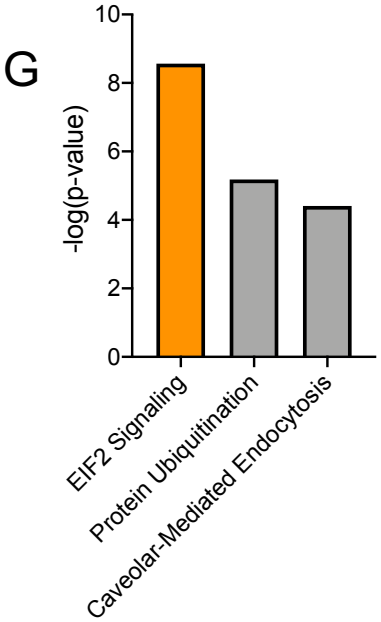
G
-log(p-value)
EIF2 Signaling
Protein Ubiquitination
Caveolar-Mediated Endocytosis

Figure 7

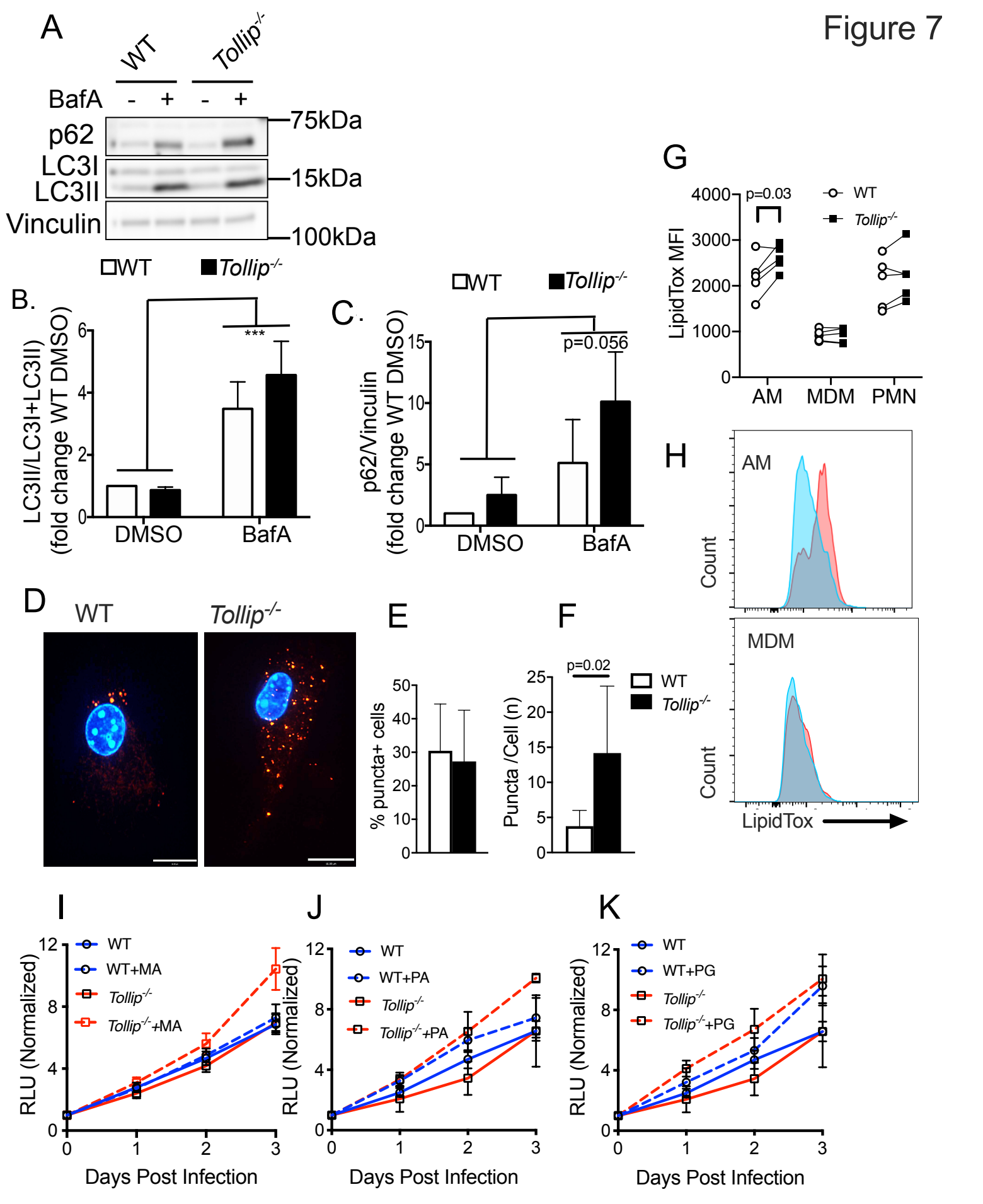
A
WT
Tollip-/-
BafA - + - +
p62
LC3I
LC3II
Vinculin
75kDa
15kDa
100kDa
WT
Tollip-/-
B.
LC3II/LC3I+LC3II) (fold change WT DMSO)
***
DMSO
BafA
C.
p62/Vinculin (fold change WT DMSO)
p=0.056
DMSO
BafA
G
p=0.03
LipidTox MFI
AM
MDM
PMN
H
AM
MDM
Count
LipidTox
D
WT
Tollip-/-
E
% puncta+ cells
F
p=0.02
Puncta /Cell (n)
I
WT
WT+MA
Tollip-/-
Tollip-/-+MA
RLU (Normalized)
Days Post Infection
J
WT
WT+PA
Tollip-/-
Tollip-/-+PA
K
WT
WT+PG
Tollip-/-
Tollip-/-+PG